Effect of Anti-COVID-19 Measures on Atmospheric Pollutants Correlated with the Economies of Medium-sized Cities in 10 Urban Areas of Grand Est Region, France

Kamill Dániel Kovács, Ionel Haidu

Article Manuscript Number SCSI-D-21-02239:

Lockdown Effect as Anti-COVID-19 Measure on Atmospheric Pollutants Revealing Economic Contributions in Medium-Sized Cities: 10 Urban Areas of Grand Est Region, France

Kamill Dániel Kovács [1, *], Ionel Haidu [1]

[1] Université de Lorraine, Laboratoire LOTERR-EA7304, Île du Saulcy, 57045 Metz, France

* Correspondence: kamill-daniel.kovacs@univ-lorraine.fr

Acknowledgments: The authors would like to thank the free software developers of QGIS and Google Earth Engine for helping our work and also to the European Environment Agency for providing the valuable station monitoring data.

Formatting of funding sources: This research did not receive any grant from funding agencies in the public, commercial, or not-for-profit sectors.

Lockdown Effect as Anti-COVID-19 Measure on Atmospheric Pollutants Revealing Economic Contributions in Medium-Sized Cities: 10 Urban Areas of Grand Est Region, France

Abstract: This study investigates with Sentinel-5P data the magnitude of the change in the concentration of air pollutants (NO_2, HCHO, SO_2, O_3, CO, and aerosol index) in the air of ten cities and urban areas of the French region of Grand Est as a result of the first lockdown imposed between 17 March 2020 - 11 May 2020. The results have shown that the air quality in the urban environments of Grand Est has improved significantly compared to the situation in 2019 in the same period without lockdown. NO_2, O_3, aerosol index and CO are the ones that were most reduced with an average of -33.98%, -5.94%, -26.82% and -0.66%, respectively (observed maximum decreases was -54.7%, -7.7%, -13.1%, and -5.3%, respectively). The largest decrease has occurred in the EPCI areas of Eurométropole de Strasbourg, CA Colmar and CA Mulhouse Alsace. It has also been seen that the greatest decreases in air pollution first occurred in land cover classes close to cities and then secondly in the built-up urban areas. In this study, a global depollution index called ACI (Atmospheric Clearance Index) has also been developed which involves several parameters of air pollution and quantitatively shows depollution–permanence of the contamination levels. In addition, the correlation between the novel ACI and other population and economic development indices has been studied. The results indicated that there is a negative and statistically significant correlation between ACI and population density, GDP, gross value added at basic prices, number of employees, and active enterprises.

Keywords: lockdown, COVID-19, air pollution, Sentinel-5P, medium-sized cities, Atmospheric Clearance Index, depollution, GDP, population density, Grand Est, France

1. Introduction

The first human cases with infection of the new SARS-CoV-2 coronavirus were reported in the municipality of Wuhan (China) at the end of 2019. The rapid spread of the

virus in a few months created a pandemic that led to the declaration of a state of health emergency in most countries (J. F. W. Chan et al., 2020; Cucinotta & Vanelli, 2020; Huang et al., 2020; WHO, 2020d). The first lockdown was imposed in Wuhan and other cities in Hubei province to stem the spread of the disease (H. Tian et al., 2020). The WHO declared the pandemic on 11 March 2020, when statistics showed more than 1 million confirmed cases in four months. By the end of 2020, 74 million confirmed cases and 1.6 million deaths from COVID-19 were recorded (WHO, 2020c).

Given the high level of spread of the virus, WHO made recommendations to implement measures against infection with the disease (WHO, 2020a). Recommendations included a 14-day quarantine for persons returning from affected areas/countries to their country of origin (WHO, 2020b). The continued rapid spread of the virus has forced the governments of countries to impose strict national lockdown measures to restrict the mobility of people, including the obligation to remain in quarantine for 14 days for those returning from certain affected areas and social estrangement (Muhammad et al., 2020). As countries implemented anti-COVID-19 measures, global economic and transport activities began to cease, which had global economic effects (Kumari & Toshniwal, 2020; Muhammad et al., 2020).

Despite the negative effects on the local and global economy, the crisis generated by COVID-19 has also brought some benefits for ecosystems and the environment: improved air quality in large cities and industrial areas, reduction of pollution in general (e.g. noise pollution), and greenhouse gases (Basu et al., 2021; Zambrano-Monserrate et al., 2020). The limitation of urban transport and long journeys, industrial activities, and construction has caused a general improvement in air quality because these anthropic activities are the major sources of air pollution (Meng et al., 2020). National lockdowns have ultimately demonstrated a viable and hitherto unique solution for the significant reduction of air pollution that seriously affects human and ecosystem health (Cameletti, 2020; Fattorini & Regoli, 2020; Lozhkina et al., 2016; Rugani & Caro, 2020; Shi & Brasseur, 2020). In

addition, studies have shown that the reduction of air pollution by lockdown measures has had a positive effect on the reduction of mortality caused by respiratory diseases (K. Chen et al., 2020; Dutheil et al., 2020; Loey et al., 2021).

This study aims to analyze changes in atmospheric concentrations of NO_2, HCHO, SO_2, O_3, CO, and aerosol index in 10 metropolitan areas of the French Grand Est region during the period of the first lockdown of 2020 compared to the same period in 2019. This region of metropolitan France has been chosen because Grand Est is an administrative territory recently created by merging three different historical regions, thus containing urban areas with varied numbers of inhabitants and economic potential, however, all its cities are medium-sized (40,000 - 300,000 inhabitants).

The methodology of the study is based on analyzing the change produced in the concentration of atmospheric pollutants during restrictions of anthropic activity, a change that is obtained by calculating the difference between satellite images and between the pollution indicators derived from satellite images that represent the levels of contamination before and during confinement in a single reference period corresponding to the first lockdown in France in 2020. The magnitude of the change that has occurred in the same period of the year but under different social and economic conditions can be obtained with this method. The data with which the change has been studied is satellite data provided by the TROPOMI sensor of the Sentinel-5P satellite. The TROPOMI sensor measures the concentration of various atmospheric pollutants using optical depth (Wei et al., 2020). Monitoring data from on-site stations have also been used while comparing satellite results with data measured on the ground.

In France, the first lockdown was imposed on 17 March 2020 and lasted until 11 May 2020. A study has shown that, in France, mobility was reduced by 79% during lockdown restrictions (Galeazzi et al., 2020) and also ceased industrial activities and secondary services. Furthermore, several studies have addressed the effect of the lockdown on air

quality in France (Ikhlasse et al., 2021; Magazzino et al., 2020; Piazzola et al., 2021; Sbai et al., 2021). The slowdown in the economy and mobility in France has also improved air quality in several urban settings, so it is important to study the effects of COVID-19 lockdown measure on medium-sized cities in France.

The objective of this study is to analyze the effectiveness of anti-COVID-19 measures to reduce air pollution in medium-sized cities (40,000 - 300,000 inhabitants) by taking into consideration the economic (GDP, GVA, employment, etc.) and social (population density) potential of urban areas. The measures taken to stop the spread of the SARS-CoV-2 coronavirus have directly affected anthropic activities also in medium-sized cities and, consequently, have indirectly modified the concentration of air pollution around these cities. Understanding the impact of severe measures applied such as the COVID-19 confinements on the reduction of air pollution is essential to be able to design environmentally sustainable and socially resilient medium-sized cities for the prevention of epidemiological/alike crises in the future.

This study contributes to the literature by emphasizing the side of the economic potential that is conditioning decontamination in medium-sized urban areas. The novelty of the study is the development of the ACI (Atmospheric Clearance Index) by comparing it with socio-economic indicators.

The major limitations of the study are the reduced availability of TROPOMI Sentinel-5P (2018-) satellite data and the small number of medium-sized cities in the Grand Est region. Further studies should be designed with a larger number of medium-sized cities and various periods when artificial restrictions on human activities were applied in those cities.

2. Literature review

Air pollution is the biggest environmental problem endangering human health and deteriorating people's quality of life (European Comission, 2017). The main pollutants that

harm human and other species' health are nitrogen dioxide (NO_2), formaldehyde (HCHO), ozone (O_3), sulfur dioxide (SO_2), carbon monoxide (CO), and respirable particulate matter ($PM_{2.5}$, PM_{10}) present in the atmosphere especially in areas of large urban and industrial agglomerations. Concentrations of NO_2, HCHO, and O_3 have temporal variations and also depend on the part of the day (Biswas et al., 2019). In addition, O_3 concentrations may be more influenced by local than regional emissions (Biswas et al., 2019). Some authors have investigated the correlation between NO_2 and COVID-19 as a decisive factor in mortality due to the new coronavirus (Ogen, 2020). The results indicated that 78% of the cases of death are in regions where there is usually a high concentration of NO_2 (Ogen, 2020). Another study found that in Italy 74% of infected people and 81% of deaths due to COVID-19 are associated with high air pollution regions (Coccia, 2021). However, it should be noted that the majority of Italy's population lives in the large urban agglomerations where there is pollution (as in other countries also where there has been a high rate of COVID-19 infection), therefore it is clear that there has been a higher infection rate in cities. Other authors have indicated that SARS viruses may stay longer in the breathable particulate material in the air (Martelletti & Martelletti, 2020), therefore there is a relationship between air pollution and infection caused by COVID-19 (Y. Zhu et al., 2020).

High O_3 concentration may be even more harmful to the health of living organisms if is influenced by local emissions (Biswas et al., 2019; Monks et al., 2015). A study examining the association between chronic exposure to environmental O_3 and cause-specific mortality in a large adult cohort has shown that long-term environmental O_3 contributes to the risk of respiratory and circulatory mortality (Turner et al., 2016).

Another source of health problems especially in urban areas is breathable particulate matter (PM). PMs less than or equal to 2.5 or 10 microns ($PM_{2.5}$, PM_{10}) are generally studied (Azimi-Yancheshmeh et al., 2021). The most important sources of $PM_{2.5}$ in the area of large cities are secondary nitrate and sulfate particles and vehicle emissions (Kim &

Hopke, 2008; Lee et al., 2018; Liang et al., 2017; Matawle et al., 2015). Other authors add that primary sources of PM also include food cooking, coal combustion in winter and by-products in summer, and, also, wood smoke (Schauer et al., 1996; Song et al., 2007; S.-P. Wu et al., 2019). Besides, $PM_{2.5}$ particles affect visibility in cities. Research has shown that sulfate is the dominant species in PM affecting light dispersion and thus visibility (Tao et al., 2009). PM particles can also contain heavy metals. The highest concentrations of heavy metals in $PM_{2.5}$ were observed during the winter in China, while the lowest concentrations of heavy metals in PM were recorded during the summer (Y. Wu et al., 2019; G. Xu et al., 2017). These investigations are important to understand the current coronavirus pandemic because fossil fuel derivatives, exposure to fine particles, metals, ultraviolet (UV) radiation, and lifestyle contribute to the immunodeficiency observed in the contemporary SARS-CoV-2 pandemic (Kumar et al., 2020; Tsatsakis et al., 2020). Urban air quality is a fundamental problem for many cities and regions in the world with various environmental, industrial, climatic, and extreme weather implications (Chatterton et al., 2000; Saito et al., 2002; She et al., 2017; H. Wang et al., 2014; W. Wang et al., 2018). Consequently, if these environmental problems of large urban agglomerations are not addressed, long-term exposure to air pollutants would not only aggravate mortality and economic consequences (Matus et al., 2012; Shen et al., 2017) but could encourage the spread of other future pandemics.

Previous studies have also addressed the relationship between pollution, economic growth and COVID-19 mortality in major urban agglomerations (Magazzino et al., 2021; Mele & Magazzino, 2021). These studies analyze how unsustainable economic growth that generates more pollution in the largest cities (New York and India, respectively) causes a higher COVID-19 death rate.

Significant changes in the concentration of air pollutants were observed since the start of national and regional lockdowns (Munir et al., 2021; Shi & Brasseur, 2020; Su et al.,

2021; Zaib et al., 2021). A consistent decrease in urban air pollution has been shown in urban areas where anti-COVID measures were taken (Cadotte, 2020; Dantas et al., 2020). In central China, concentrations of $PM_{2.5}$, PM_{10}, SO_2, CO, and NO_2 decreased during February 2020 with 46.5%, 48.9%, 52.5%, 36.2% and 52.8%, respectively, compared to February of the previous years (K. Xu, Cui, Young, Hsieh, et al., 2020; K. Xu, Cui, Young, Wang, et al., 2020). In India, decreases in $PM_{2.5}$, PM_{10}, CO and NO_2 concentrations were observed of 43%, 31%, 10%, and 18%, respectively, during the lockdown period compared to previous years (Sharma et al., 2020). The same trend was observed in other densely populated areas and other authors also highlight the spatial effects (Kerimray et al., 2020; Nakada & Urban, 2020). Research in five European countries (United Kingdom, Spain, Northern Italy, France, and Sweden) has shown that industrial and mobility activities were lower in the lockdown period in 2020 and as a result, pollution emissions of NO_2, $PM_{2.5}$, PM_{10} were reduced by approximately 20-40% (Skirienė & Stasiškienė, 2021). Research for Western Europe has indicated NO_2 concentration decreases of 30-50% and PM decreases of 5-15% in Western European countries (Menut et al., 2020). Significant reductions of $PM_{2.5}$, PM_{10}, SO_2 and NO_2 occurred in Poland also in some cities (up to 26.4%, 33.9%, 23%, 19%, respectively) (Filonchyk et al., 2020). Other studies have focused on the reduction of CO_2 emissions due to the lack of mass traffic during the lockdown period (X. Tian et al., 2021). Effects of lockdown on air pollution reduction (NO_2 and PM_{10}) have also been observed with national air quality monitoring data in Portugal or Spain (Baldasano, 2020; Gama et al., 2021). Others have pointed out that the restriction of cars has caused changes in concentrations of $PM_{2.5}$ and PM_{10} with 39.3% and 31.4% in 49 cities in China (Z. Chen et al., 2021).

However, urban air pollution has been modified, consciously reduced by other events also in years prior to COVID-19. An example is the 2008 Olympic Games in Beijing when urban traffic emissions of volatile organic compounds (VOCs), CO, nitrogen oxides (NOx),

and PM_{10} were reduced by 55.5%, 56.8%, 45.7%, and 51.6%, respectively, compared to before the Games (Zhou et al., 2010). Another example is the commemorative activities celebrated in Beijing in 2015, where the restrictions of urban traffic led to reductions of NO_2 concentration from 40% to 46.2% (Cheng et al., 2018).

3. Study area and materials

3.1. Study area

The study area covers ten urban areas that currently belong to the French Grand Est region (Fig. 1). The Grand Est region is one of the thirteen metropolitan regions of mainland France that, together with the overseas territories make up the eighteen regions of the French Republic. Its capital is the Alsatian city of Strasbourg. The Grand Est region is an artificial administrative creation for the territorial reform of 2014 that merges the diverse historical regions of Alsace, Lorraine, and Champagne-Ardennes. The creation of the region came into force in 2016. Therefore, culturally there is no historical connection in the region because it is divided between two areas with different cultural features: an area of Latin

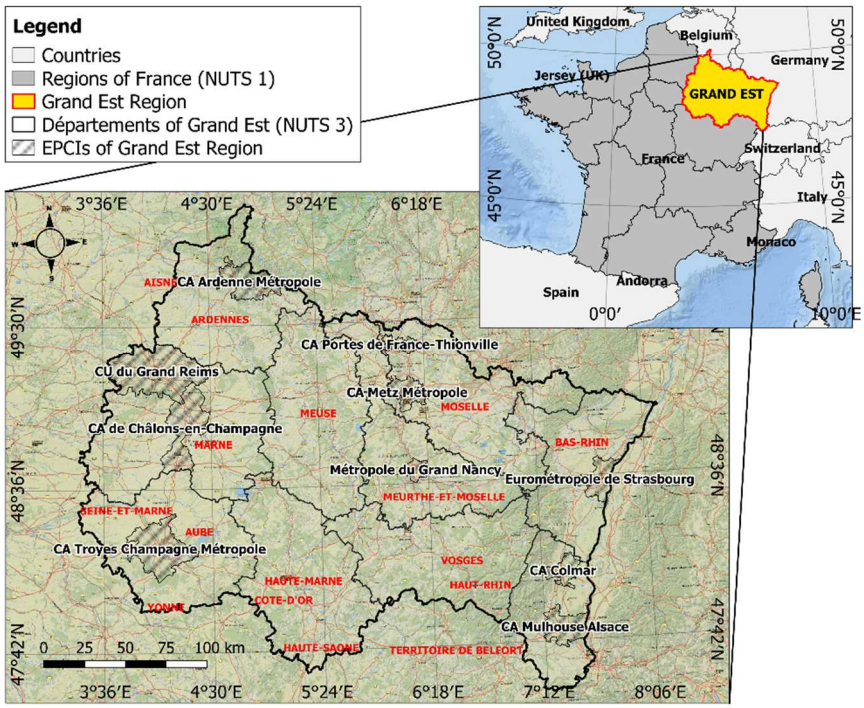

Figure 1. Location of the Grand Est Region and the EPCIs

tradition (Champagne-Ardennes) and another area of Germanic tradition (Alsace and Moselle).

The ten urban areas are the cities of Charleville-Mézière – Sedan, Colmar, Châlons-en-Champagne, Metz, Mulhouse, Thionville, Troyes, Reims, Strasbourg and Nancy. The administrative area of these urban areas studied corresponds to the French EPCI (Établissement public de coopération intercommunale). A public institution for inter-municipal cooperation (EPCI, Établissement public de coopération intercommunale) is a French administrative structure that brings together several municipalities to exercise some of their common competences (Vie Publique, n.d.-a, n.d.-b). The names of the ten EPCIs are: CA Ardenne Métropole, CA Colmar, CA de Châlons-en-Champagne, CA Metz Métropole, CA Mulhouse Alsace, CA Portes de France-Thionville, CA Troyes Champagne Métropole, CU du Grand Reims, Eurométropole de Strasbourg and Métropole du Grand Nancy. Urban areas were chosen according to population and importance criteria in the region. In principle, cities with more than 40,000 inhabitants were chosen.

3.2. Data used

The data used in this study are satellite data from Sentinel-5P. The Sentinel-5P was launched in 2017. The satellite sensor is known as TROPOMI. The satellite instrument of the Sentinel-5 Precursor mission collects global data for air quality assessment. The TROPOMI instrument is a multispectral sensor that records the reflectance of significant wavelengths to measure atmospheric concentrations of ozone, methane, formaldehyde, aerosol, carbon monoxide, nitrogen oxide, and sulfur dioxide, as well as the characteristics of clouds at a spatial resolution of 0.01 arc degrees (ESA - Copernicus, n.d.-b).

This study investigated the change in atmospheric concentrations of pollutants of nitrogen dioxide (NO_2), formaldehyde (HCHO), sulfur dioxide (SO_2), ozone (O3), carbon monoxide (CO), and UV aerosol index (Kovács, 2021d).

In the case of nitrogen dioxide (NO_2), the tropospheric column concentration closest to the surface has been investigated. Sentinel-5P provides data on total, tropospheric, and stratospheric NO_2 concentration. Nitrogen dioxide enters the atmosphere as a result of anthropogenic activities such as the combustion of fossil fuels and the burning of biomass but also contributes to natural processes including microbiological processes in the soil, forest fires, or lightning. NO is converted to NO_2 and vice versa in the presence of sunlight by a photochemical cycle involving ozone (O_3) (Aggarwal & Toshniwal, 2019; Brewer et al., 1973; Peel et al., 2013). The process passes on a timescale of minutes. TROPOMI sensor NO_2 data is available from 2018-06-28 to date.

In the case of formaldehyde, tropospheric column concentration has also been used. Formaldehyde (HCHO) is an intermediate gas in nearly all non-methane volatile organic compound oxidation chains (NMVOCs), which eventually leads to the emergence of CO. HCHO sources include vegetation, fire, traffic and industrial-chemical activities (ESA - Copernicus, n.d.-b). Seasonal and interannual variations in the distribution of HCHO are mainly related to temperature changes and fire events, but it should be noted that they also depend on changes in anthropogenic activities (Luecken et al., 2012, 2018; L. Zhu et al., 2016). Sentinel-5P HCHO data is available from 2018-10-02 to date.

The atmospheric SO_2 concentration is available in columnar concentration. SO_2 can enter the Earth's atmosphere through both natural and anthropogenic processes, although most are of anthropogenic origin (about 70%). SO_2 emissions negatively affect human health and air quality and also have a negative effect on climate change through radiative forcing because they form sulfate aerosols in the atmosphere (ESA - Copernicus, n.d.-b). The largest sources of SO_2 emissions are the burning of fossil fuels in power plants and other industrial facilities (Aas et al., 2019; United States Environmental Protection Agency, 2019; Z. Wang et al., 2018). TROPOMI sensor SO_2 data is available from 2018-07-10 to date.

This study investigates also the concentration of O_3 in the atmospheric column. Ozone is a gas that protects the biosphere and living things from ultraviolet (UV) solar radiation from space. In the troposphere, it acts as an effective cleaning agent, however, O_3 in high concentrations becomes harmful to the health of humans, animals, and vegetation. O_3 is also a greenhouse gas that contributes to climate change (Brenna et al., 2019; Luecken et al., 2018; Zhang et al., 2019). Available O_3 data from the Sentinel-5P are available from 2018-07-10 to date.

Atmospheric CO is available in columnar concentration. CO is an important atmospheric gas that contributes to the chemical processes that occur in the troposphere. The main sources of CO are fossil fuel combustion, biomass burning and atmospheric oxidation of methane and other hydrocarbons (Badr & Probert, 1994; Conte et al., 2019; Robbins et al., 1968). While fossil fuel combustion is the main source of CO in the northern mid-latitudes, in the tropics, isoprene oxidation and biomass burning are essential. TROPOMI on the Sentinel 5 Precursor satellite (S5P) observes the global abundance of CO by taking advantage of Earth radiance measurements in clear and cloudy skies in the 2.3 µm spectral range of the short-wave infrared (SWIR) part of the solar spectrum. The CO columns have absolute sensitivity to the tropospheric boundary layer thanks to the TROPOMI clear-sky observations. For cloudy atmospheres, the sensitivity of the column changes according to the path of light (ESA - Copernicus, n.d.-b). Sentinel-5P CO data is available from 2018-06-28 to the current date.

UV Aerosol Index is a measure calculated through the total columnar concentration. The UV Aerosol Index (UVAI) of the Sentinel-5P TROPOMI is a measurement of aerosol prevalence in the atmosphere that may be ideal for detecting the evolution of episodic aerosols of varied origin. Also called "Absorbing Aerosol Index (AAI)" (Go et al., 2017; Hammer et al., 2016). The AAI index is calculated based on wavelength-dependent changes in Rayleigh dispersion in the UV spectral range for a pair of wavelengths. The difference

between observed and modeled reflectance is the AAI index. High positive AAI index values indicate a high presence of ultraviolet absorbing aerosols, such as desert dust and fire smoke, while low and negative values indicate less presence of aerosols. A lower value of -2.10 AAI indicates the absence of aerosols (ESA - Copernicus, n.d.-b). The aerosol index data of the TROPOMI sensor are available from 2018-07-04 to the present date.

All atmospheric variables in the Sentinel-5P, except for Methane (CH4), have two types of data. One is called "Near Real-Time (NRTI)" and the other is "Offline (OFFL)". CH4 data is available in the Offline (OFFL) version. The difference between the two data versions is that NRTI covers a smaller area than OFFL, but appears more quickly after the acquisition, thus reflecting the near real-time situation of the spatial distribution. On the other hand, the OFFL version contains data from a single orbit, which contains data for just one hemisphere since half of the Earth is dark. Taking into account these characteristics and differences between NRTI and OFFL data, in this study, the research was done by choosing the version "Near Real-Time (NRTI)" of the Sentinel-5P data.

Meteorological data from satellites were also used to study meteorological conditions (temperature, total precipitation, dewpoint, atmospheric pressure at sea level, atmospheric pressure at surface level, wind u and v components, wind speed, humidity and solar radiation). These data were retrieved using Google Earth Engine from ERA5 (ECMWF re-analysis) (Copernicus Climate Change Service, n.d.; Earth Engine Data Catalog, n.d.-b; Kovács, 2021a), GLDAS-2.1 (Earth Engine Data Catalog, n.d.-c; Kovács, 2021c; NASA GES DISC at NASA Goddard Space Flight Center, n.d.), and ERA5-Land (Earth Engine Data Catalog, n.d.-a; ESA - Copernicus, n.d.-a; Kovács, 2021b), which have similar spatial resolution (0.25 arc degrees, 0.25 arc degrees, and 0.1 arc degrees, respectively).

For the validation of the satellite data, monitoring data from stations located in the cities of Grand Est have been used. These data come from the European Environment

Agency (EEA) database (European Environment Agency (EEA), 2020; European Environment Agnecy (EEA), 2020).

In addition, statistical data related to the population and economic development of the ten urban areas of Grand Est were used. These data come from the Eurostat database (Eurostat, n.d.).

4. Methodology

The working method of this study is to model the change in the atmospheric concentration of some pollutants (NO_2, HCHO, SO_2, O_3, CO, and AAI) during the lockdown period by the coronavirus. This change is calculated from satellite column density data measured between two dates marking the lockdown period in which certain measures to stop the spread of coronavirus were applied. Column density is a term that in this case refers to a total amount per unit area of a material suspended in the atmosphere, measured along the length of a column. As previously mentioned, the data of the Sentinel-5P have its beginning from the date 2018-11-22 T12:00:13, therefore, the period of comparison is limited to the year 2019.

The detection of the change in air pollutants produced by the application of anti-COVID measures was made by calculating the arithmetic difference between the standings of 2020 and 2019 taking into account the same reference period that is March 17 - May 11. The purpose of this method was to eliminate temporary effects that may contribute to the concentration of certain air pollutants.

The stages of the research investigating the socio-environmental magnitude of the change in metropolitan and urban areas are eight: (1) definition of the reference period according to the anti-COVID lockdown measures, (2) obtaining and downloading NO_2 raster, SO_2, CO, HCHO, O_3, and aerosol index according to the reference period established for the year 2020 and applied for the year 2019, (3) calculation of the arithmetic differences between the 2020 and 2019 rasters, (4) representative sampling from the difference raster

for change distribution modeling, (5) reclassification of the Corine Land Cover soil cover raster version 2018 to four categories for modeling the change produced in the land cover categories (Water, Built-up, Vegetation, Bare soil), (6) elimination of seasonal meteorological factors with homogeneity analysis, (7) creation of an overall decontamination index reflecting the change of the 6 pollution parameters, (8) study of the correlation between the depollution index and other population and economic development indices (Fig. 2).

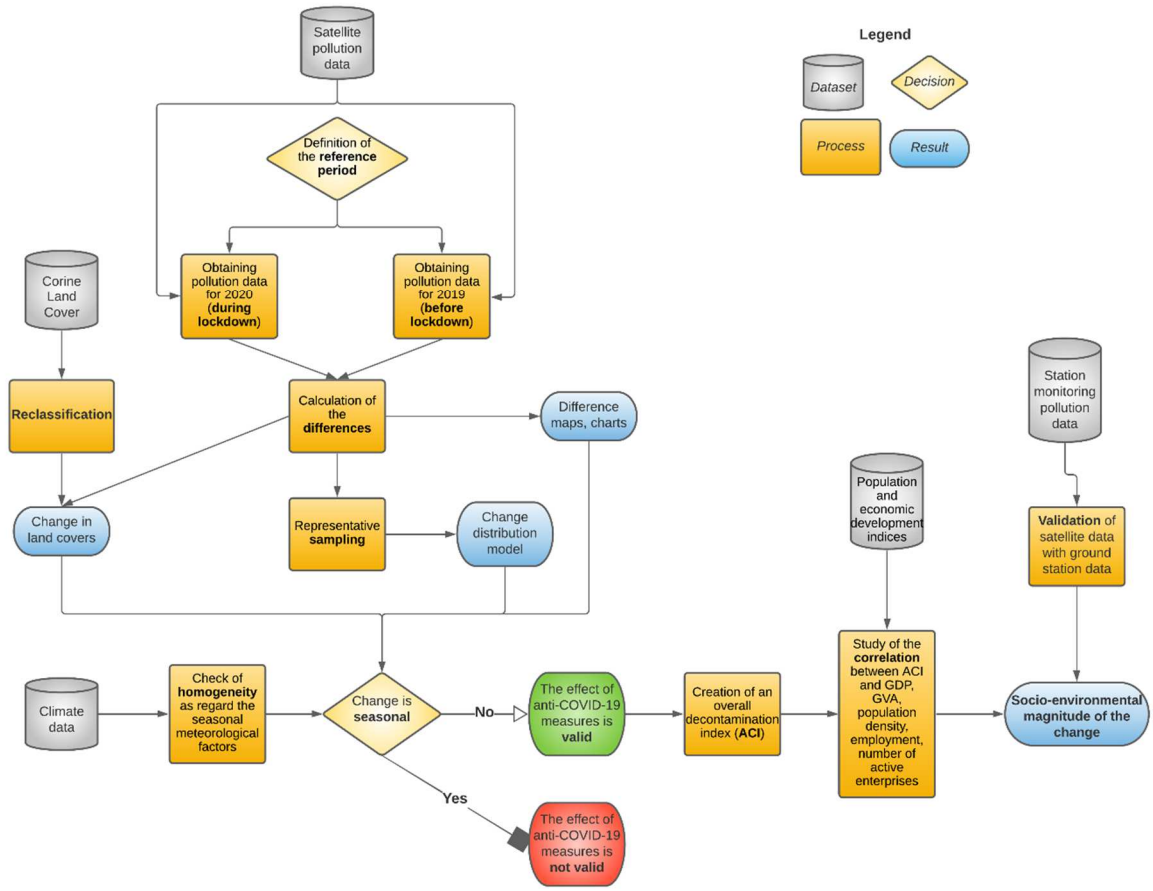

Figure 2. Workflow of the methodology. The flowchart reflects the succession of the work steps

The definition of the reference period was established taking into account the steps taken by the French government and the local administration to stop the spread of the virus. The reference period of this study corresponds to the first lockdown phase in France, which was generalized for the ten metropolitan areas that have been investigated in this study. Therefore, the dates covering this period are 17 March 2020 and 11 May 2020. This same period of days (56 days) was applied for the raster in the filter of 2019.

Obtaining and downloading the NO_2, SO_2, CO, HCHO, O_3, and aerosol index was done using the Google Earth Engine application. The original Sentinel 5P Level 2 (L2) data is grouped by time, not by latitude and longitude. In order for satellite data to be entered into Google Earth Engine, each Sentinel 5P product at Level L2 becomes Level 3 (L3) by conversion. This is done by keeping a single grid per orbit, in other words, no aggregation is done between the products. The original products that encompass antimeridian are ingested as two Earth Engine assets, with the suffixes _1 and _2. The conversion to Level 3 (L3) is carried out using the *harpconvert* tool through the *bin_spatial* operation, in this way the satellite products can be processed with other HARP-type commands through code lines. Therefore, the filtering of the satellite data was done with code lines in Earth Engine.

Google Earth Engine allows to call the COPERNICUS/S5P/NRTI satellite database and perform date filters (.filterDate()), spatial extension filters (.filterBounds(AOI)) and represent the data using statistical methods such as min(), max(), mean(), etc. In this case, the representation of pixel values was made with .median(). The data for each variable is represented by selecting (.select()) the raster band containing the tropospheric or numerical column density information. Representation over a given geographical area (AOI) requires the use of a clip layer that delimits the study area (.clip(AOI)). Finally, the download is done by exporting the same raster with the command Export.image.toDrive(). The code is available at the following address (requires a registered Google Earth Engine account): https://code.earthengine.google.com/e9fcf98c03da3200892cace2d6cf15be (Kovács, 2021d).

The calculation of the arithmetic differences between the 2020 and 2019 rasters was performed using the QGIS raster calculator. Therefore, the arithmetic difference between the pixel value of 2020 and 2019 shows where it has decreased (negative value) and where it has increased (positive value) the concentration of the given atmospheric pollutant. Using the original data and the difference data obtained, three types of results were generated:

maps and difference graphs, comparison of distributions, and representation of differences within the categories of soil cover.

Representative samples were taken from the difference rasters in order to model the magnitude of the distribution of the change. The number of representative samples was calculated with the finite sample size calculation equation (Eq. 1) (Darling & Robbins, 1967). The population size (N) is considered as the totality of the pixels that cover the study area (9010457 pixels). Therefore, the sample size searched with a margin of error of 5% is 385 observation samples.

$$n = \frac{N * Z_{\alpha}^{2} * p * q}{e^{2} * (N - 1) + Z_{\alpha}^{2} * p * q} \quad (1)$$

where $\boldsymbol{n}$ is the size of the sample sought, $\boldsymbol{N}$ is the size of the population or universe, $\boldsymbol{Z\alpha}$ is the statistical parameter that depends on the confidence level, e is the accepted maximum estimation error, $\boldsymbol{p}$ is the probability that the event studied occurs and $\boldsymbol{q = (1 - p)}$ which is the probability that the event will not happen.

Representative sampling was done with the help of the *Point Sampling Tool* available as a plugin in QGIS. In the first instance, a random point layer has been created with 385 elements. The *Point Sampling Tool* plugin collects the pixel values of each layer (raster layer) and attributes it to the same point that corresponds to the underlying pixel. For an adequate representation of the distribution of the data, boxplots have been used and minimum and maximum observed data on the whole raster have also been included.

For modeling of the change produced in the different categories of soil cover within the metropolitan areas of Grand Est the CLC classification (2018) has been reclassified into four representative categories: "Water", "Built-up (Urban)", "Agricultural/Vegetation" and “Bare soil" (Table 1). The category "Bare soil" could not be established in this study because within the study area of the metropolitan areas of Grand Est the soil classes corresponding to this proposed category were not found (Fig. A.9). The statistical tool *Raster layer zonal statistics* available in QGIS has been used to represent the average

difference produced in the land cover categories within the different metropolitan areas of the region.

Table 1. Reclassification of CLC code values

CLC 2018 class	Reclassified value and Name
111 – 142	2 [Built-up (Urban)]
211 – 324	3 [Agricultural/Vegetation]
331 – 335	4 [Bare soil]
411 – 523	1 [Water]

The elimination of seasonal meteorological factors has been performed by homogeneity analysis of meteorological data with chi-square test ($\chi 2$). For this purpose, daily data were obtained for each EPCI urban area between 17 March and 11 May for 9 meteorological factors that may influence the concentration of pollution. The 9 factors are: temperature, total precipitation, dew point, atmospheric pressure at sea level, atmospheric pressure at surface level, wind u and v components, wind speed, humidity and solar radiation. These data come from three satellite products: ERA5 (ECMWF re-analysis), GLDAS-2.1, and ERA5-Land, with similar spatial resolution (0.25 arc degrees, 0.25 arc degrees, and 0.1 arc degrees, respectively). In the case of the GLDAS-2.1 and ERA5-Land products, the native data is hourly data so the wind speed, humidity and solar radiation data were averaged into days.

The homogeneity analysis investigates whether two different distributions can be considered equal (H_0 = homogeneity) or not (unequal) (H_1 = difference). In our case the two distributions that were analyzed were the distribution of the meteorological factor data in the period of March 17 – May 11 in 2019 and the distribution of the same meteorological factor in the same period in 2020 that corresponds to lockdown. So on with the 9 meteorological factors studied. In this way we have checked the distribution similarity of the lockdown period data with the data for the same period without lockdown in the previous year. The chi-square statistical test ($\chi 2$) for homogeneity is defined as follows (Eq. 2):

$$\chi_h^2 = nm \sum_{i=1}^{r} \frac{\left(\frac{v_i}{n} - \frac{\mu_i}{m}\right)^2}{v_i + \mu_i} \quad (2)$$

where **vi** are the observations of the first distribution, **μi** are the observations of the second distribution, **n** is the total number of observations of the first distribution and **m** is the total number of observations of the second distribution. In our case the total number of observations was 56 (days) in both distributions. The codes from which these meteorological data were obtained are available at the following links; ERA5 (ECMWF re-analysis): https://code.earthengine.google.com/c8e51091665cc4eb409b69614bac5ffc (Kovács, 2021a), GLDAS-2.1: https://code.earthengine.google.com/7f9d0346778cab602e3d31eb5dabbc5f (Kovács, 2021c), y ERA5-Land: https://code.earthengine.google.com/8c65acb73c7850625a1e06960c082d9f (Kovács, 2021b).

The creation of an overall depollution index has been carried out to cover the six pollution parameters studied in a single index that reflects the total magnitude of the loss and permanence of air pollution in the ten urban areas of Grand Est. The depollution index has been called "Atmospheric Clearance Index" (ACI). The ACI has been calculated in the first instance by standardizing the pixel values of the NO_2, HCHO, SO_2, O_3, CO and AAI difference rasters between 2019 and 2020, and then adding the standardized difference rasters. The resulting raster is an index in which negative values show decontamination levels and positive values show levels of permanence of air pollution. The standardization of pixel values has been done with the SAGA Tool Grid Standardization tool. The result of standardization is a score (z) which is calculated as the gross score (x) minus the arithmetic mean of the raster (m), divided by the standard deviation of the raster (s), and multiplied by a defined stretching factor (d) (Conrad et al., 2015) (Eq. 3):

$$z = d * (x - m)/s \quad (3)$$

Therefore "Atmospheric Crearance Index" (ACI) is defined as the sum of standardized difference records (Eq. 4):

$$ACI = Z_{dNO_2} + Z_{dHCHO} + Z_{dSO_2} + Z_{dO_3} + Z_{dCO} + Z_{dAAI} \quad (4)$$

where **d** is the difference raster and **Z** is the standardized raster. The result is a raster in which values range from higher negative values to higher positive values. Negative values show the intensity of decontamination (loss) and positive values show the intensity of permanence of air pollution.

The study of the correlation between the ACI index and population density, GDP, gross value added (GV), number of employees and active enterprises has been carried out to see if there is any relationship between the decline-permanence of air pollution allegedly caused by the lockdown, and other factors of population and economic development. The t-test for the correlation coefficient has been performed with the following equation (Eq. 5):

$$t_{r_{xy}} = \frac{r_{xy}\sqrt{n-2}}{\sqrt{1-r_{xy}^2}} \quad (5)$$

where $\mathbf{r_{xy}}$ is the correlation coefficient and **n** is the sample size. The null hypothesis (H_0) of the test is $\rho=0$ and the alternative (H_1) hypothesis is $\rho\neq0$.

5. Results

5.1. Comparison of data distributions: representative sample of NO_2, HCHO, SO_2, O_3, CO, and AAI rasters for 2019 and 2020

Changes in the distributions of air pollutants (NO_2, HCHO, SO_2, O_3, CO, and AAI) show very different trends. The concentration of NO_2 in the urban regions of the Grand Est

has decreased in 2020 with an average of -1.9E-05 mol/m^2 compared to 2019 (see Fig. 3a, Fig. 4a).

The change in HCHO concentrations has been very diverse in urban areas of the region. In the cities of Grand Est, the concentration of HCHO in the air has generally increased in most of these urban regions with an average of 1.1E-05 mol/m^2. It should also be noted that despite this trend of general increase there are areas where atypically there were much more notable declines (around -1.0E-04 mol/m^2) (see Fig. 3b, Fig. 4b).

The spatial distribution of SO_2 follows the same upward trend as HCHO. The concentration of SO_2 in the cities of Grand Est has increased by 2020 with 3.4E-05 mol/m^2. Also, in the case of the change in SO_2 concentration in urban air, areas with significant decreases were identified (-7.0E-04 mol/m^2) (see Fig. 3c, Fig. 4c).

The level of concentration of O_3 in urban air shows notable decreases in the largest urban agglomerations of the Grand Est. O_3 has been reduced overall with -0.01 mol/m^2. We can say that the O_3 in the urban air of these cities has decreased significantly (see Fig. 3d, Fig. 4d).

CO follows the same trend as HCHO and SO_2 with minimal changes by 2020. However, the loss of CO concentration in the air is significant in the cities of the Grand Est. There is a decrease of -2.0E-04 mol/m^2. It should also be noted here that, despite the slight increase in the urban region, there are areas with a significant decrease (-0.002 mol/m^2) (see Fig. 3e, Fig. 4e).

The aerosol index (AAI) also shows very significant decreases in the cities of the Grand Est region. An average aerosol loss of -0.3 AAI is recorded (see Fig. 3f, Fig. 4f).

5.2. Comparison of average changes in urban areas of NO_2, HCHO, SO_2, O_3, CO, and AAI in 2019 and 2020

In the case of the concentration of NO_2, there are exclusively concentration losses in the urban air of the cities of Grand Est (Fig. 5a). In 2019 we have an average value of 5.8E-05

mol/m^2 that drops in 2020 to 3.8E-05 mol/m^2 (loss of -2.0E-05 mol/m^2, decrease with -33.98%). The highest NO_2 drop is recorded at the Eurométropole in Strasbourg at -3.3E-05 mol/m^2, followed by CA Mulhouse Alsace (-3.1E-05 mol/m^2) and CA Colmar (-2.9E-05 mol/m^2). The maximum observed decrease of NO_2 is -54.7%.

In the case of the concentration of HCHO, cities with increase and loss of HCHO in the urban environment are recorded (Fig. 5b). In the cities belonging to Grand Est, the average in 2019 was 5.9E-05 mol/m^2 which amounted to 6.7E-05 mol/m^2, obtaining a HCHO gain of 7.7E-06 mol/m^2 (an increase of 13.03%). Declines were recorded in the areas of CA Portes de France-Thionville (-7.6E-06 mol/m^2) and Eurométropole de Strasbourg (-6.7E-06 mol/m^2). The greatest increase in HCHO is observed in CA Troyes Champagne Métropole (1.7E-05 mol/m^2), CA Ardenne Métropole (1.6E-05 mol/m^2) and CA Colmar (1.4E-05 mol/m^2).

The concentration of SO_2 in urban air tends to increase in most of the 10 localities (Fig. 5c). In the case of the cities of Grand Est, the average SO_2 was increased from 1.0E-04 mol/m^2 to 1.5E-04 mol/m^2, assuming a gain of 4.8E-05 mol/m^2 (an increase of 47.76%) in the air. The urban areas where the concentration of SO_2 is declining are Eurométropole de Strasbourg (-3.7E-05 mol/m^2), CU du Grand Reims (-3.1E-06 mol/m^2) and CA de Châlons-en-Champagne (-2.9E-05 mol/m^2). The highest average increase is recorded in CA Portes de France-Thionville (1.8E-04 mol/m^2).

At global level, HCHO and SO_2 are introduced to the atmosphere by several different sources from the burning of fuels by power plants, extraction of metals from the ore to vehicle emissions. On the other hand, formaldehyde is ubiquitous in the environment with variations depending on local industrial emissions or traffic. Although the zonal statistics show an increase in HCHO and SO_2 in various EPCIs of the Grand Est, the increase in the concentration of these gases is not directly associated with urban areas because isolated areas of increase appear outside the cities (Fig. 3b, Fig. 3c, compare with Fig. A9). In

addition, large cities with greater anthropic impact such as Strasbourg and Reims have registered a decrease in HCHO and/or SO_2 concentration, which indicates that the increase is not associated with urban anthropic activity.

The concentration of O_3 has decreased in all the urban areas studied in the Grand Est (Fig. 5d). Cities as a whole show O_3 losses: from the average 0.17 mol/m^2 in 2019, the concentrations fell to 0.16 mol/m^2 in the reference period of 2020 (decrease of -5.94%). The largest decline of O_3 in urban air was recorded in the areas of CA Troyes Champagne Métropole (-0.011 mol/m^2) and CA Ardenne Métropole (-0.011 mol/m^2). The maximum observed decrease of O_3 is -7.7%.

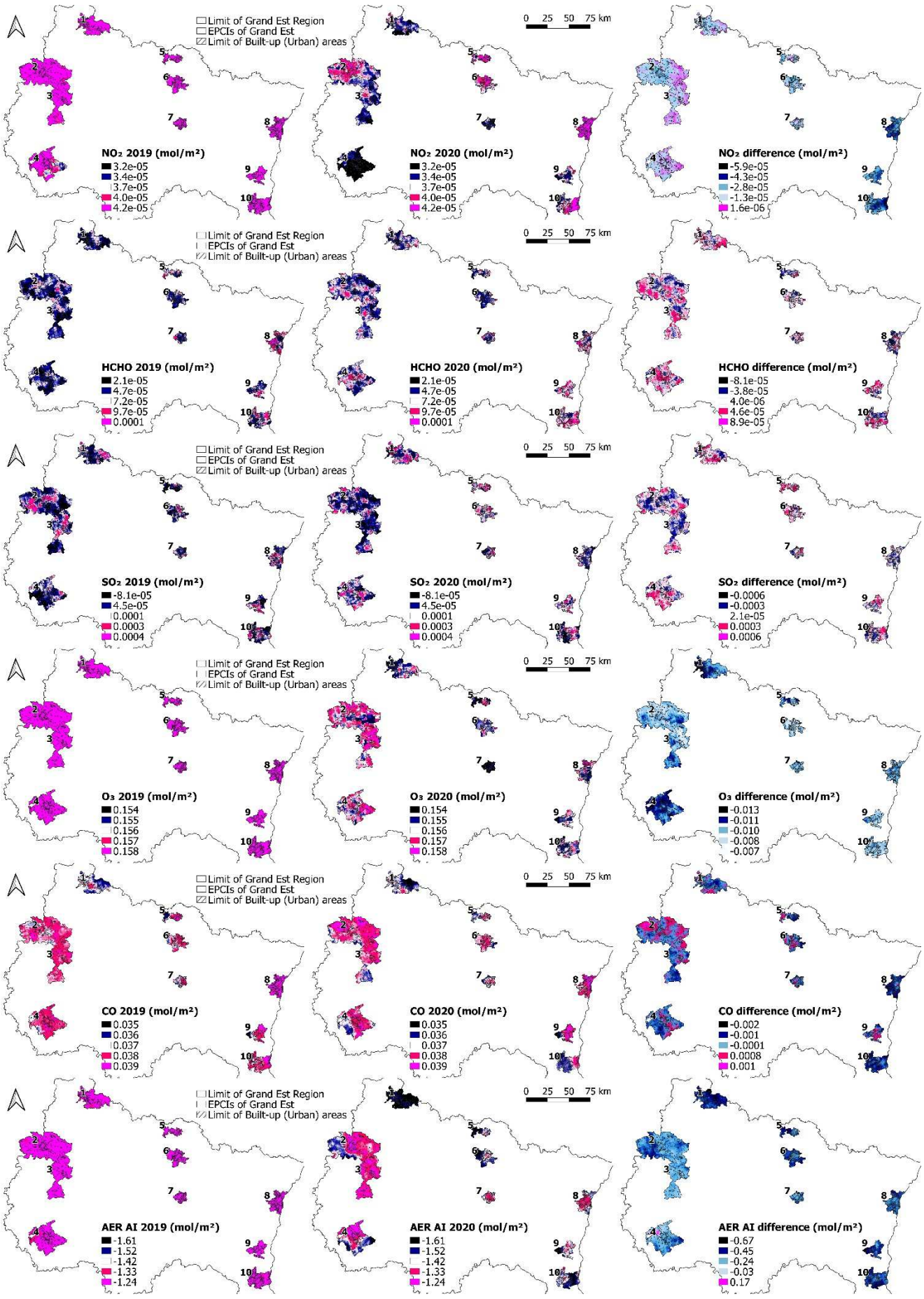

Figure 3. Spatial distribution of the concentration of air pollutants in the EPCIs of Grand Est in 2019 and 2020 (March 17 – May 11) (rows from top to bottom **a–f**): NO_2, HCHO, SO_2, O_3, CO, AER AI / AAI). The enumeration of the EPCI corresponds to: (**1**) CA Ardenne Métropole, (**2**) CU du Grand Reims, (**3**) CA de Châlons-en-Champagne, (**4**) CA Troyes Champagne Métropole, (**5**) CA Portes de France-Thionville, (**6**) CA Metz Métropole, (**7**) Métropole du Grand Nan[illegible]) Eurométropole de Strasbourg, (**9**) CA Colmar, (**10**) CA Mulhouse Alsace.

a

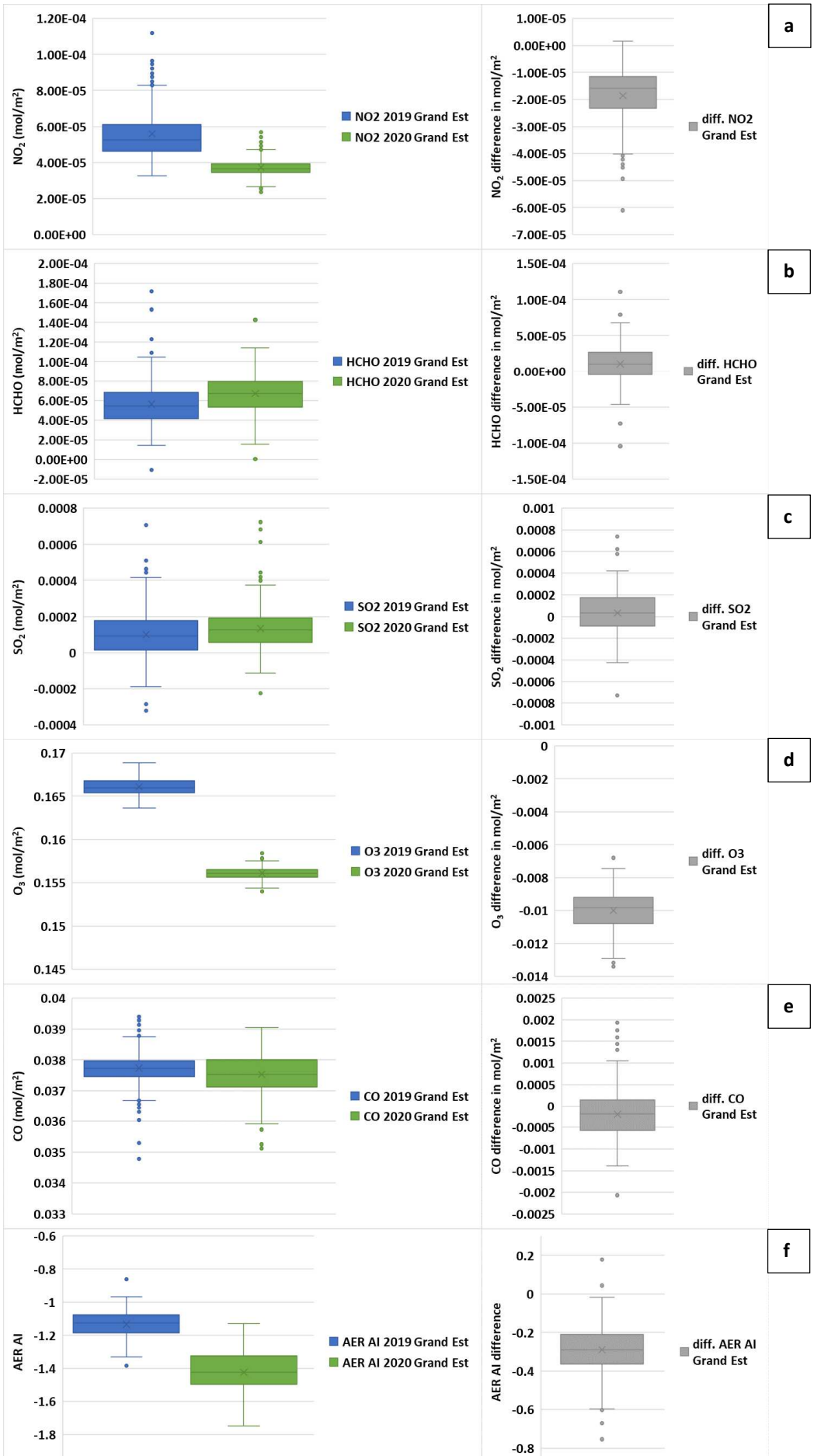

Figure 4. Comparison of data distribution with representative sampling of NO_2 (**a**), HCHO (**b**), SO_2 (**c**), O_3 (**d**), CO (**e**), and AER AI / AAI (**f**) rasters in the reference period between March 17 – May 11 in 2019 (without lockdown) and 2020 (with lockdown).

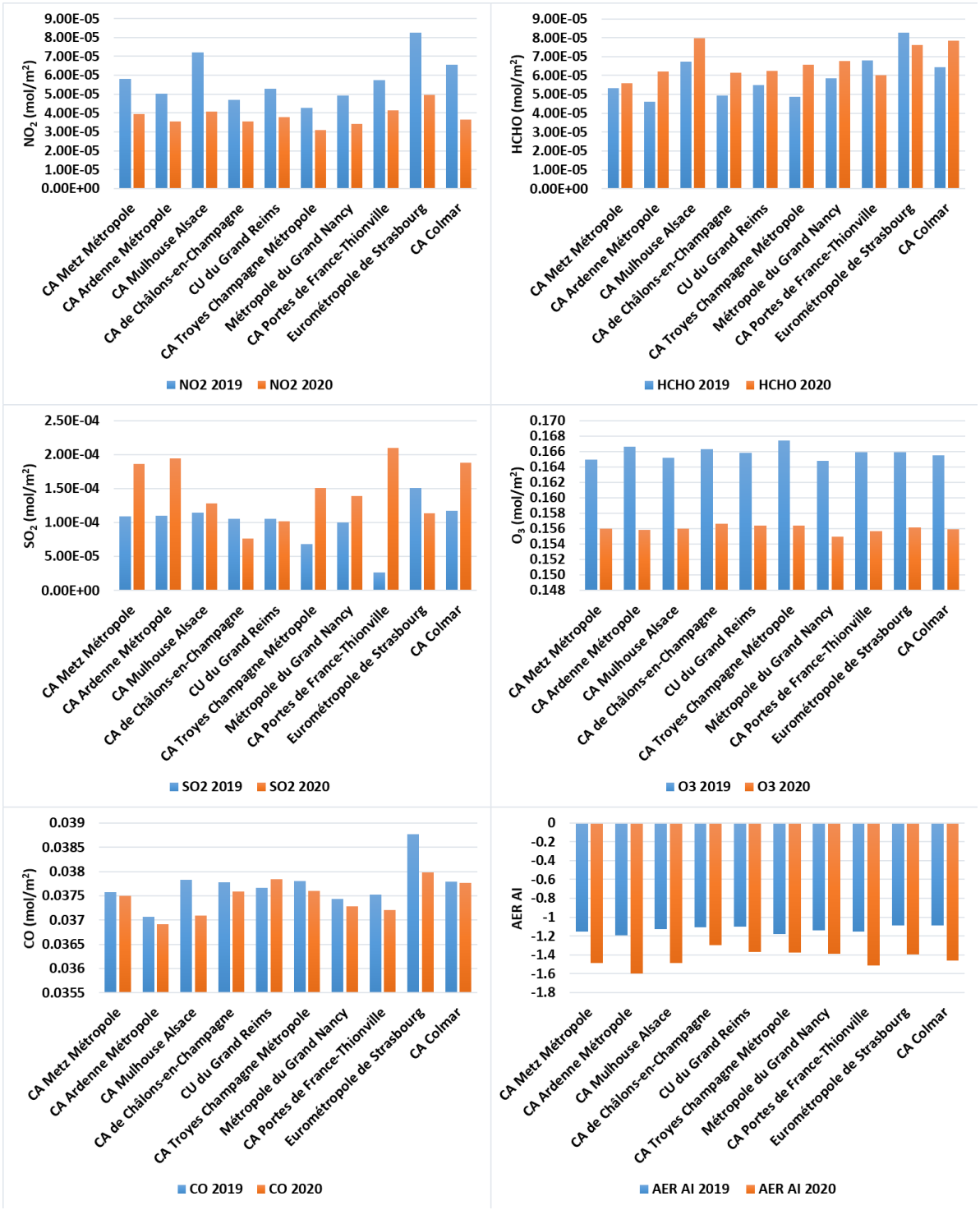

Figure 5. Comparison of average concentration of NO_2 (**a**), HCHO (**b**), SO_2 (**c**), O_3 (**d**), CO (**e**), and AER AI / AAI (**f**) in the Grand Est EPCIs between March 17 – May 11 in 2019 (without lockdown) and 2020 (with lockdown).

a

b

CO is the atmospheric pollutant that remained almost constant in the urban areas of the Grand Est (Fig. 5e). A slight decrease is observed in the set of cities of Grand Est where from the 0.038 mol/m^2 in 2019 the concentration of CO reduced to 0.037 mol/m^2 in the reference period of 2020 (decrease of -0.66%). The most significant decline in CO concentration was recorded in the Eurométropole areas of Strasbourg (-7.9E-04 mol/m^2) and CA Mulhouse Alsace (-7.3E-04 mol/m^2). The most significant increase is observed in CU du Grand Reims (1.8E-04 mol/m^2). The maximum observed decrease of CO is -5.3%.

The aerosol index (AAI) shows that the concentration of suspended aerosol particles in the air of the urban environment had a significant reduction (Fig. 5f). In all the cities of Grand Est, the decrease is of -0,30 AAI (in the year 2019 the average was -1.13 AAI that was reduced in the period of 2020 to -1.44 AAI, a decrease of -26.82%). The most significant drop in aerosols is in the urban area of CA Ardenne Métropole (-0.41 AAI). However, significant average declines are also observed in CA Colmar (-0.38 AAI), CA Mulhouse Alsace (-0.36 AAI), CA Portes de France-Thionville (-0.36 AAI) and CA Metz Métropole (-0.33 AAI). The maximum observed decrease of AAI is -13.1%.

5.3. Comparison of the average difference in land covers

In the case of the cities of Grand Est, all land cover categories report a decrease of NO_2 (Fig. 6a). The categories with the highest descent are "Built-up (urban)" (-2.1E-05 mol/m^2) and "Water" (-2.1E-05 mol/m^2), followed by "Vegetation" (-1.6E-05 mol/m^2). The most significant decrease in the category "Water" is recorded in CA Mulhouse Alsace (-4.1E-05 mol/m^2), followed by Eurométropole de Strasbourg (-3.2E-05 mol/m^2) and CA Colmar (-2.8E-05 mol/m^2). In the "Built-up (Urban)" category, the largest NO_2 decrease also occurs in CA Mulhouse Alsace (-3.3E-05 mol/m^2), followed by Eurométropole de Strasbourg (-3.2E-05 mol/m^2) and CA Colmar (-2.9E-05 mol/m^2). In the "Vegetation" category the first area as far as the magnitude of the decrease is Eurométropole de Strasbourg (-3.4E-05 mol/m^2), followed by CA Mulhouse Alsace (-3.1E-05 mol/m^2) and CA Colmar (-2.9E-05

mol/m^2). Consequently, the largest reduction in the concentration of NO_2 occurred in the urban areas of Eurométropole in Strasbourg, CA Mulhouse Alsace, and CA Colmar.

HCHO has a diverse behavior in terms of land cover categories and areas of the Grand Est. In the Grand Est region in general, the increase in the concentration of HCHO in urban air predominates (Fig. 6b). In cities and metropolitan areas in general there is an increase in all classes. The largest increase is in the category "Vegetation" (1.0E-05 mol/m^2), followed by "Built-up (Urban)" (7.8E-06 mol/m^2) and "Water" (2.6E-06 mol/m^2). Despite the general trend of increase, average values of decrease are recorded in some cases in urban areas. For example, in the "Water" category the most significant decline of HCHO occurred in CA Colmar (-1.3E-05 mol/m^2), followed by CA Metz Métropole (-6.3E-06 mol/m^2). On the other hand, the greatest increase is recorded in CA Troyes Champagne Métropole (1.4E-05 mol/m^2) and CA Portes de France-Thionville (9.9E-06 mol/m^2). In the category "Built-up (Urban)" the greatest decrease is observed in Eurométropole de Strasbourg (-2.1E-06 mol/m^2), and another case of descent is CA Metz Métropole (-2.8E-07 mol/m^2). On the other hand, the most significant increase is observed in CA Troyes Champagne Métropole (2.3E-05 mol/m^2) and CA Ardenne Métropole (2.0E-05 mol/m^2). In the category "Vegetation" the cases that recorded a decrease in HCHO are Eurométropole de Strasbourg (-1.0E-05 mol/m^2) and CA Portes de France-Thionville (-1.0E-05 mol/m^2). The most notable increase in this class occurred in CA Troyes Champagne Métropole (1.7E-05 mol/m^2) and CA Ardenne Métropole (1.6E-05 mol/m^2). Consequently, the metropolitan areas inclined to HCHO drop in air are Eurométropole de Strasbourg and CA Metz Métropole, while CA Troyes Champagne Métropole and CA Ardenne Métropole were more likely to increase HCHO.

SO_2 has different behavior in terms of the magnitude of the change in the land cover categories and urban areas of Grand Est. In the cities of Grand Est in general an increase is observed in all categories (Fig. 6c). The greatest increase is recorded in the "Vegetation"

(3.5E-05 mol/m^2), followed by "Built-up (Urban)" (7.4E-06 mol/m^2) and "Water" (6.1E-06 mol/m^2). In the "Water" category the most significant descent is observed in CA de Châlons-en-Champagne (-1.0E-04 mol/m^2), followed by Eurométropole de Strasbourg (-7.1E-05 mol/m^2), CA Mulhouse Alsace (-3.2E-05 mol/m^2) and CA Troyes Champagne Métropole (-1.8E-05 mol/m^2). The largest increase of SO_2 in this category is recorded in CA Portes de France-Thionville (2.4E-04 mol/m^2). In the category "Built-up (Urban)" the most significant decline of the SO_2 occurred in the Eurométropole area of Strasbourg (-6.4E-05 mol/m^2), however, important decreases are also recorded in CU du Grand Reims (-5.5E-05 mol/m^2), CA Mulhouse Alsace (-4.2E-05 mol/m^2) and CA of Châlons-en-Champagne (-3.8E-05 mol/m^2). On the other hand, the largest increase of SO_2 is in CA Portes de France-Thionville (2.0E-04 mol/m^2), followed by CA Ardenne Métropole (1.3E-04 mol/m^2). In the category "Vegetation" the most important descent occurs in CA de Châlons-en-Champagne (-2.8E-05 mol/m^2) and Eurométropole de Strasbourg (-1.4E-05 mol/m^2). The other metropolitan areas registered an increase, the highest being in CA Portes de France-Thionville (1.8E-04 mol/m^2). Therefore, in the case of the SO_2 we have four zones with an inclination to the loss of SO_2: in the first place CA de Châlons-en-Champagne, Eurométropole de Strasbourg, CU du Grand Reims and CA Mulhouse Alsace. The CA Portes areas of France-Thionville, CA Ardenne Métropole, and the other cities of Grand Est have recorded average increases in their land categories.

The concentration of O_3 in urban air shows a decrease in all parts of the Grand Est. In the case of the Grand Est cities in all categories of soil cover, a decrease of O_3 is observed (Fig. 6d). The greatest concentration loss is recorded in the "Water" class (-0.01 mol/m^2), followed by "Vegetation" (-0.0099 mol/m^2) and "Built-up (Urban)" (-0.0098 mol/m^2). In the coverage category "Water" the highest drop was observed in CA Troyes Champagne Métropole (-0.0114 mol/m^2), followed by CA Ardenne Métropole (-0.0108 mol/m^2). In the category "Built-up (Urban)" the most notable decrease occurred in CA Ardenne Métropole

(-0.0111 mol/m^2) and in CA Troyes Champagne Métropole (-0.0110 mol/m^2), too. Similarly, in the "Vegetation" category, the metropolitan areas of CA Troyes Champagne

Métropole (-0.0110 mol/m^2) and CA Ardenne Métropole (-0.0107 mol/m^2) stand out in terms of the decrease in O_3. Consequently, the largest O_3 drop in urban air occurred in the

metropolitan areas of CA Troyes Champagne Métropole and CA Ardenne Métropole.

The CO concentration also has a different behavior according to the land cover

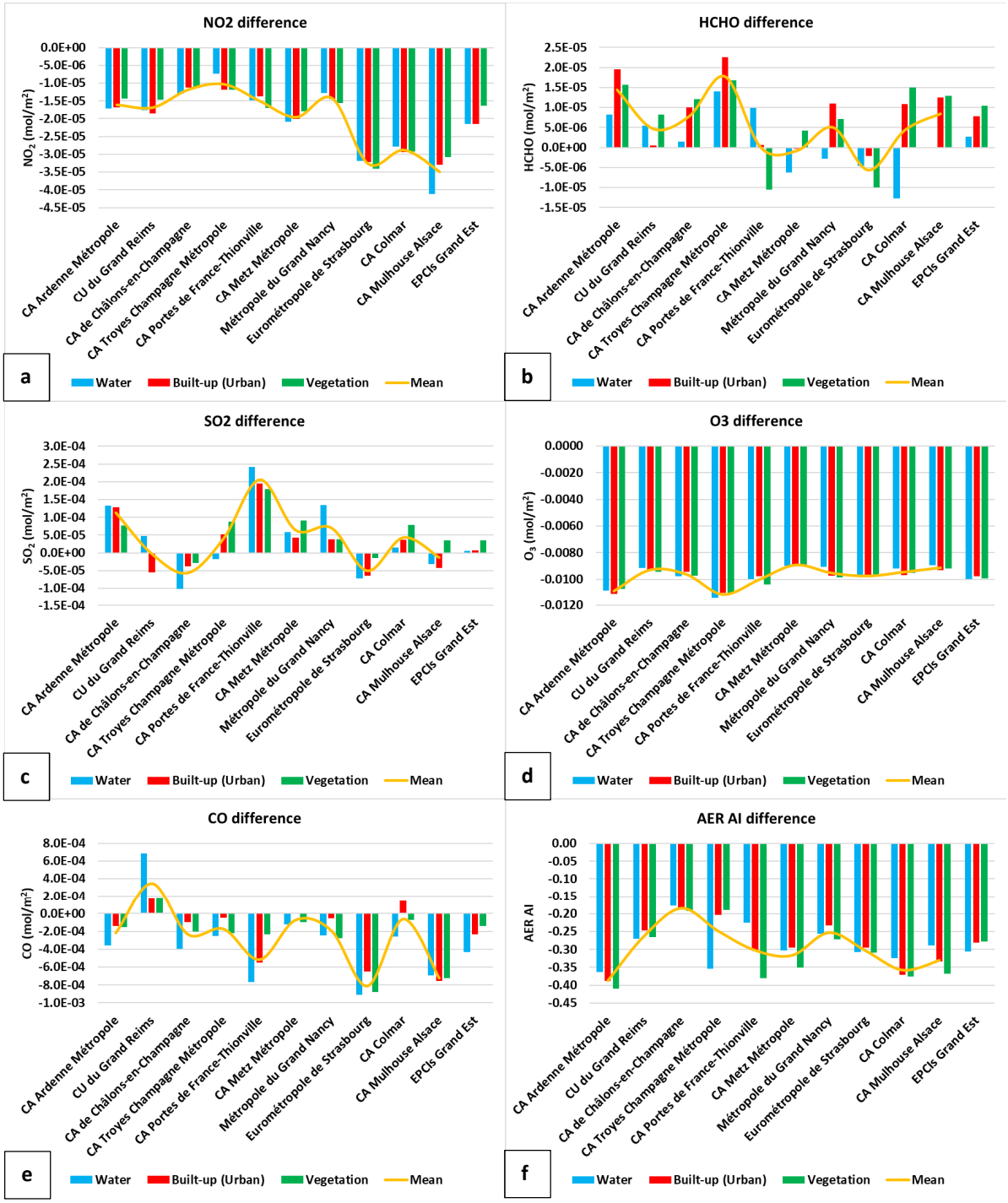

Figure 6. Comparison of changes between 2019 and 2020 in the reference period (March 17 – May 11) of the concentration of NO_2 (**a**), HCHO (**b**), SO_2 (**c**), O_3 (**d**), CO (**e**), and AER AI / AAI (**f**) in the categories of land covers in the EPCIs of Grand Est.

categories. In the cities and urban areas of Grand Est, there is an overall average decline in CO in all established classes (Fig. 6e). The greatest decrease is recorded in the class "Water" (-4.3E-04 mol/m^2), followed by "Built-up (Urban)" (-2.3E-04 mol/m^2) and "Vegetation" (-1.4E-04 mol/m^2). However, there are metropolitan areas where the different categories of land cover recorded increases in CO. Starting with the decrease in CO, the area where the most significant decrease in the "Water" class is observed is Eurométropole de Strasbourg (-9.1E-04 mol/m^2), followed by CA Portes de France-Thionville (-7.7E-04 mol/m^2) and CA Mulhouse Alsace (-6.9E-04 mol/m^2). The only increase in this category is recorded in CU du Grand Reims (6.9E-04 mol/m^2). The coverage category "Built-up (Urban)" follows the same pattern in terms of CO decrease: in first place are CA Mulhouse Alsace (-7.6E-04 mol/m^2), followed by Eurométropole de Strasbourg (-6.5E-04 mol/m^2) and CA Portes de France-Thionville (-5.5E-04 mol/m^2). Three areas registered an increase in CO: CU du Grand Reims (1.7E-04 mol/m^2), CA Colmar (1.5E-04 mol/m^2) and CA Metz Métropole (7.8E-07 mol/m^2). Significant declines in the "Vegetation" category occurred at Eurométropole de Strasbourg (-8.8E-04 mol/m^2) and CA Mulhouse Alsace (-7.2E-04 mol/m^2). The only case with an increase in CO is CU du Grand Reims (1.8E-04 mol/m^2). Therefore, the three metropolitan areas where CO has decreased most significantly in the categories of land cover are Eurométropole de Strasbourg, CA Mulhouse Alsace, and CA Portes de France-Thionville. The only metropolitan area in which the CO had an increasing behavior is CU du Grand Reims.

The concentration of aerosols also has a generally significant average decreasing behavior in most land cover categories (Fig. 6f). In the case of the cities and metropolitan areas of Grand Est, the greatest decrease is recorded in the class "Water" (-0.31 AAI), followed by the classes "Built-up (Urban)" and "Vegetation" (-0.28 AAI, respectively). In the "Water" category the greatest decrease in aerosol concentration is recorded in CA Ardenne Métropole (-0.36 AAI), followed by CA Troyes Champagne Métropole (-0.35

AAI) and CA Colmar (-0.32 AAI). In the ground cover category "Built-up (Urban)" the most significant decline is again observed in CA Ardenne Métropole (-0.39 AAI), followed by CA Colmar (-0.37 AAI) and CA Mulhouse Alsace (-0.33 AAI). In the category "Vegetation" the metropolitan areas with the most important descents are: CA Ardenne Métropole (-0.41 AAI), CA Colmar (-0.38 AAI) and CA Portes de France-Thionville (-0.38 AAI). As a result, the Grand Est metropolitan areas where the reduction in aerosols in the urban environment has been greatest are CA Ardenne Métropole, CA Colmar, CA Mulhouse Alsace and CA Metz Métropole.

5.4. Elimination of seasonal meteorological factors: homogeneity analysis with chi-square (χ2) test

Homogeneity analysis with chi-square test (χ2) investigates whether two data distributions are equal or not. The peer distributions that were checked were meteorological parameters for the period 17 March - 11 May 2019 and 2020 for the ten urban areas of Grand Est separately. The parameters studied were temperature, total precipitation, dewpoint, atmospheric pressure at sea level, atmospheric pressure at surface level, wind u and v components, wind speed, humidity and solar radiation. This analysis was important to perform to see if can be removed these meteorological factors that together can influence the concentration of air pollution (Yang et al., 2019).

The result has shown that almost all peer distributions are homogeneous, i.e., they do not differ statistically significantly from each other at the probability level of $p<0.01$. There have only been five cases in which some meteorological parameter showed significant difference: the u component of the wind in the case of CU du Grand Reims, the dewpoint in CA Troyes Champagne Métropole, the humidity in CA Colmar, the dewpoint and humidity in CA Mulhouse Alsace (Table A.1).

5.5. Atmospheric Clearance Index (ACI), a global depollution index

The ACI raster results from the sum of the difference rasters before and during lockdown with standardized values involved as contamination parameters. Negative values indicate where and at what magnitude the depollution phenomenon has occurred. On the other hand, positive values show where and at what magnitude air pollution has remained in

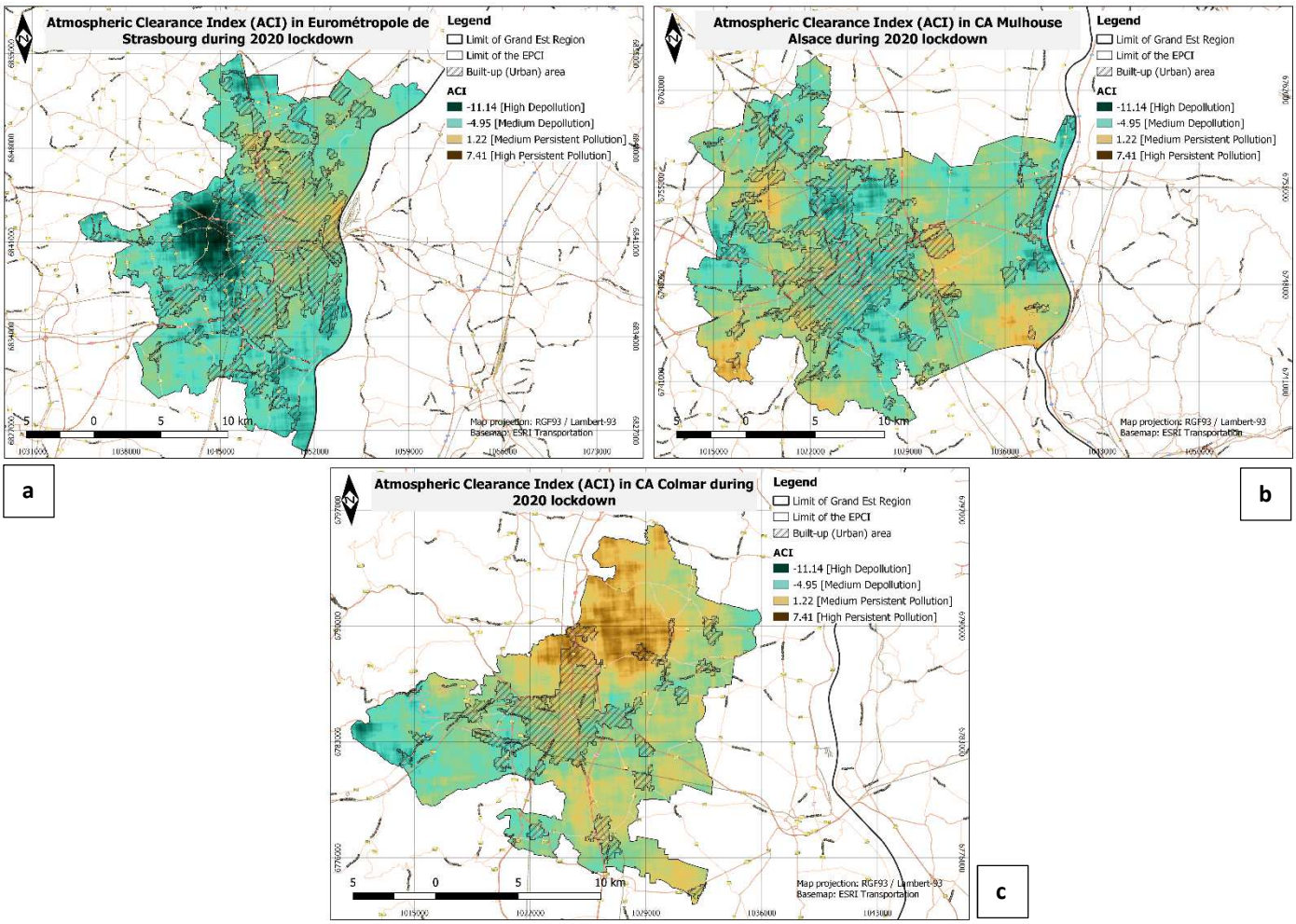

Figure 7. Atmospheric Clearance Index (ACI) in (**a**) Eurométropole de Strasbourg, (**b**) CA Mulhouse Alsace, and (**c**) CA Colmar

urban areas (Fig. 7, Figs. A.2-A.8).

The ACI index shows that the greatest depollution has occurred in the agglomerations of the cities of Strasbourg, Mulhouse and Colmar. There have also been high levels of depollution in the areas of CA Ardenne Métropole and CA Portes de France-Thionville (Fig. 8). The highest level of permanence of contamination is observed in CA Châlons-en-Champagne, followed by CU du Grand Reims and CA Troyes Champagne Métropole.

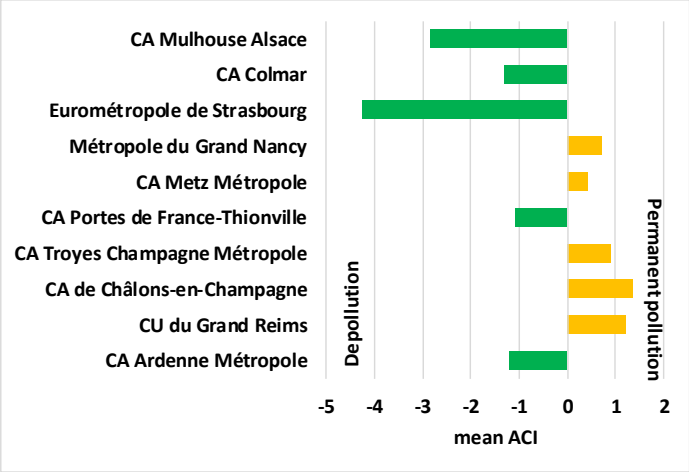

Figure 8. Mean Atmospheric Clearance Index (ACI) in major Grand Est Urban Areas

5.6. Correlation between ACI and population density, GDP, GVA, number of employees, and number of active enterprises in major urban areas of Grand Est

The correlation between ACI and population density, GDP, gross value added (GVA), number of employees, and number of active enterprises has been studied to see if there is any relationship between the level of depollution-permanence of pollution and other population index or economic development level.

The strongest correlation was observed between ACI and population density (r=-0.84), whose coefficient of determination (r^2=0.70) reveals that ACI is largely explained with the level of population density (Fig. 9a). The t-test for the correlation coefficient has shown that this relationship is statistically significant: t(8) = -4.36, p<0.05, H1. The curve that was used

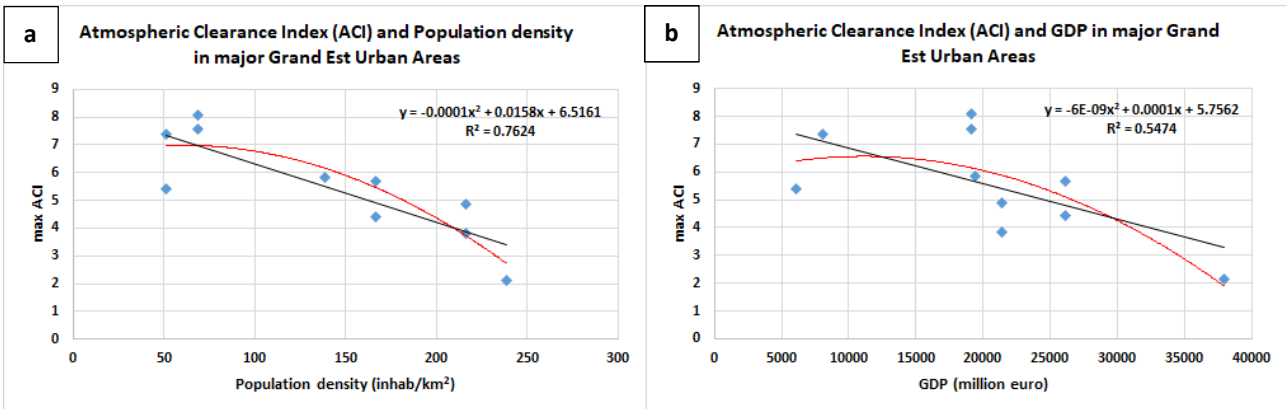

Figure 9. Scatterplot between (**a**) ACI and population density, and (**b**) ACI and GDP

to describes the points is a polynomial curve of degree 2.

There is also a strong correlation between ACI and other economic indicators. For example, the correlation coefficient between ACI and GDP is r=-0.63, whose coefficient of

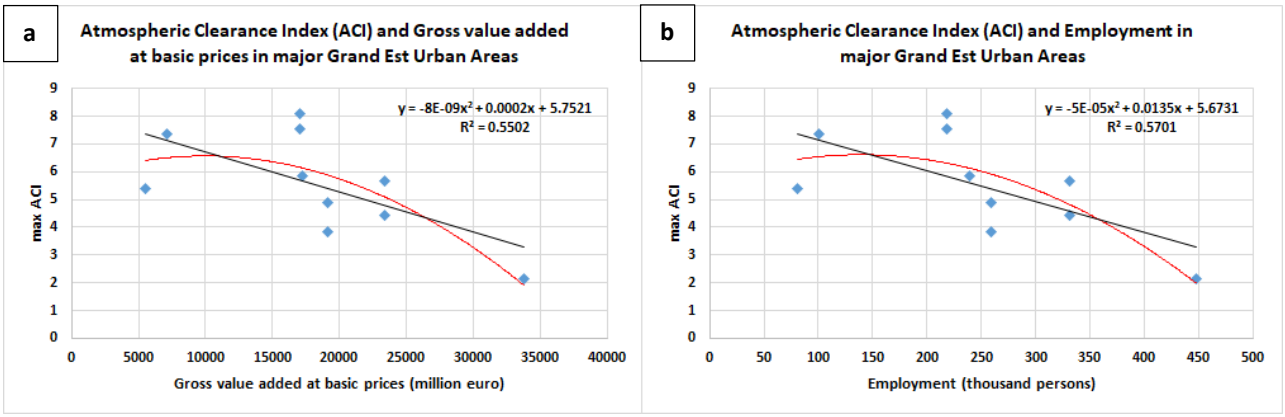

Figure 10. Scatterplot between (**a**) ACI and gross value added at basic prices, and (**b**) ACI and employment

determination is r^2=0.40. The t-test for this correlation coefficient has also shown that it is statistically significant: t(8) = -2.31, p<0.05, H1. Similarly, the curve that was used to suit the points is the polynomial of degree 2 (Fig. 9b).

The correlation coefficient between ACI and gross value added at basic prices (GVA) is r=-0.63, with a coefficient of determination of r^2=0.40. This correlation is also statistically significant: t(8) = -2.31, p<0.05, H1. The degree 2 polynomial curve is also well adapted here to describe the points (Fig. 10a).

The correlation coefficient between ACI and the number of employees reveals another inverse proportionality relationship between depollution levels and economic development (r=-0.66). The coefficient of determination in this case is r^2=0.43. The test t for is correlation coefficient also showed that the relationship is statistically significant: t(8) = -2.45, p<0.05, H1 (Fig. 10b).

The correlation coefficient between ACI and the population of active enterprises in t - number is also strongly of inverse proportionality: r=-0.74, with a coefficient of determination of r^2=0.54. The t-test for

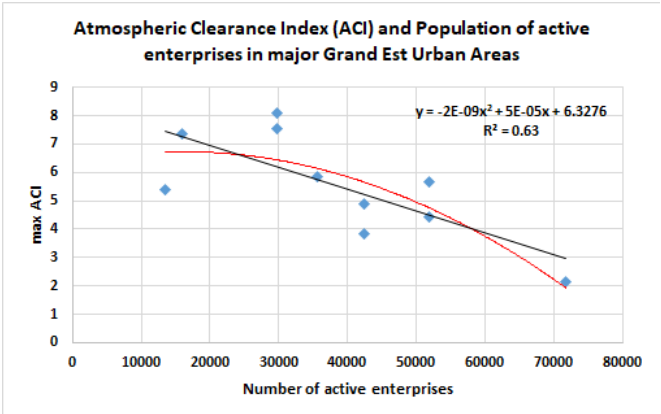

Figure 11. Scatterplot between ACI and active enterprises

this correlation coefficient has also shown that this relationship is statistically significant: $t(8) = -3.08$, $p<0.05$, H1 (Fig. 11). The enterprises taken into consideration belong to the sectors of industry, construction and services, except insurance activities of holding companies.

6. Discussion

Previous studies that analyzed the relationship between air pollution, GDP, and COVID-19 mortality and infection addressed the side of pollution that is conditioned by the level of economic growth studied exclusively with the GDP measure (Magazzino et al., 2021; Mele & Magazzino, 2021). However, this study investigates the level of decontamination expressed by an index (ACI) designed for this purpose, and it has been discovered that there is an inverse correlation between decontamination caused by anti-COVID-19 measures and various socio-economic indices (GDP, GVA, density population, number of employees and number of active companies).

Other studies that have exclusively used on-site monitoring data in cities (Baldasano, 2020; Gama et al., 2021; Ikhlasse et al., 2021; Skirienė & Stasiškienė, 2021), emphasize only the magnitude of the decrease in NO_2, $PM_{2.5}$, PM_{10} and other pollutants, and do not show what relationship there is between the decrease caused by the application of restrictive measures and the intensity of the socio-economic activity in those cities. In addition, there are studies that analyzed the change produced by the anti-COVID-19 measures with satellite data (K. L. Chan et al., 2021; Cheng et al., 2018), however, they do not address medium-sized cities or only focus on a large area of urban agglomeration (Dantas et al., 2020; Nakada & Urban, 2020; Su et al., 2021).

In this study, it has been observed that SO_2 and HCHO gases have increased in the surroundings of cities despite the anti-COVID-19 measures applied (47.76% and 13.03%, respectively). Similarly, the increase in SO_2 concentration under lockdown measures has been observed by Higham et al. (2021) in Great Britain where SO_2 levels have doubled

during the enforcement of containment measures. In contrast, other authors have confirmed that both SO_2 and HCHO have decreased in the atmosphere in other parts of the world (Javed et al., 2020; Nguyen et al., 2021). It is possible that the increase in SO_2 and HCHO in some cities of the Grand Est is due to an imbalance in the chemistry of the air near the surface in which a change in the distribution of gases occurred as an indirect effect of lockdown measures. The imbalance may have been exacerbated by the change in the concentration of the other atmospheric pollutants and by meteorological conditions at particularly low humidity levels (Higham et al., 2021). Furthermore, the climate type of the Grand Est region according to the Köppen–Geiger classification is the same oceanic west coast marine climate (Cfb) as in Great Britain. Other authors add that SO_2 tends to vary in large cities (Q. Wang & Li, 2021).

6.1. Validation of satellite data with meteorological data

The behavior of the concentration of air pollution in the urban areas of Grand Est during the lockdown by COVID-19 has been diverse. There have been areas with significant decreases in pollution, but other areas have remained with levels of pollution. The concentration of NO_2, O_3, CO and AAI has had an overall decreasing trend in all urban areas. On the other hand, the concentration of HCHO and SO_2 has shown a tendency of permanence and even increase, but it should also be noted that in these cases there have also been significant decreases in some urban areas. The increase of HCHO and SO_2 in the air is due to several contributing factors to the phenomenon because its sources are numerous and vary according to geographical space.

The concentration of NO_2 has decreased in all ten urban areas. The greatest decline in NO_2 has occurred in the metropolitan areas of Strasbourg, Mulhouse and Colmar, which are the most industrialized areas, with the greatest economic potential and most densely populated. The concentration of HCHO has generally increased, however, there have been two urban areas where it has been observed a decrease: CA Portes de France-Thionville and

Eurométropole de Strasbourg. Both areas are highly developed economically. The same trend is observed in the case of SO_2 also: permanence and increase in general, but there are three urban areas with reduced pollution. These areas are, again in first place, Eurométropole de Strasbourg followed by CA Châlons-en-Champagne and CU du Grand Reims. The cities of Reims and Châlons-en-Champagne are another economic pole in the western part of the Grand Est region. The concentration of O_3 and aerosols decreased in all ten urban areas. The CO also declined most noticeably in the cities of Strasbourg and Mulhouse. Therefore, taking into account these changes in the pollution parameters separately, it can be stated that the three urban areas that experienced the greatest decrease in air pollution were Strasbourg, Mulhouse and Colmar.

It has also been seen through the different categories of land use that the decreases in pollution in urban areas mainly correspond to the immediate proximity or to the built-up area itself (Fig. A.9, Fig. 6). This means that the phenomenon of reduction is due to the fact that the sources of pollution associated with the cities were reduced by the application of the anti-COVID-19 measures.

In spite of all these observations it could not be said with certainty that the observed decreases in the parameters of pollution are to a large extent due to the anti-COVID-19 adopted by the French authority until a thorough and detailed analysis of the meteorological conditions has been carried out. This analysis was carried out taking into account 9 meteorological factors that together can greatly influence pollution concentrations. The homogeneity analysis with the chi-square test of meteorological data in the same reference period (17 March - 11 May) in the years 2019 and 2020 has shown that the meteorological conditions were very similar in the two different years, that is, in 2020 when anti-COVID measures were applied and in 2019 when there was no health emergency in the same reference period (Fig. 12, Table 2). As a result, the observed decreases cannot have been

influenced by the temporal variation of weather conditions but by the measures taken in the context of the SARS-CoV-2 pandemic.

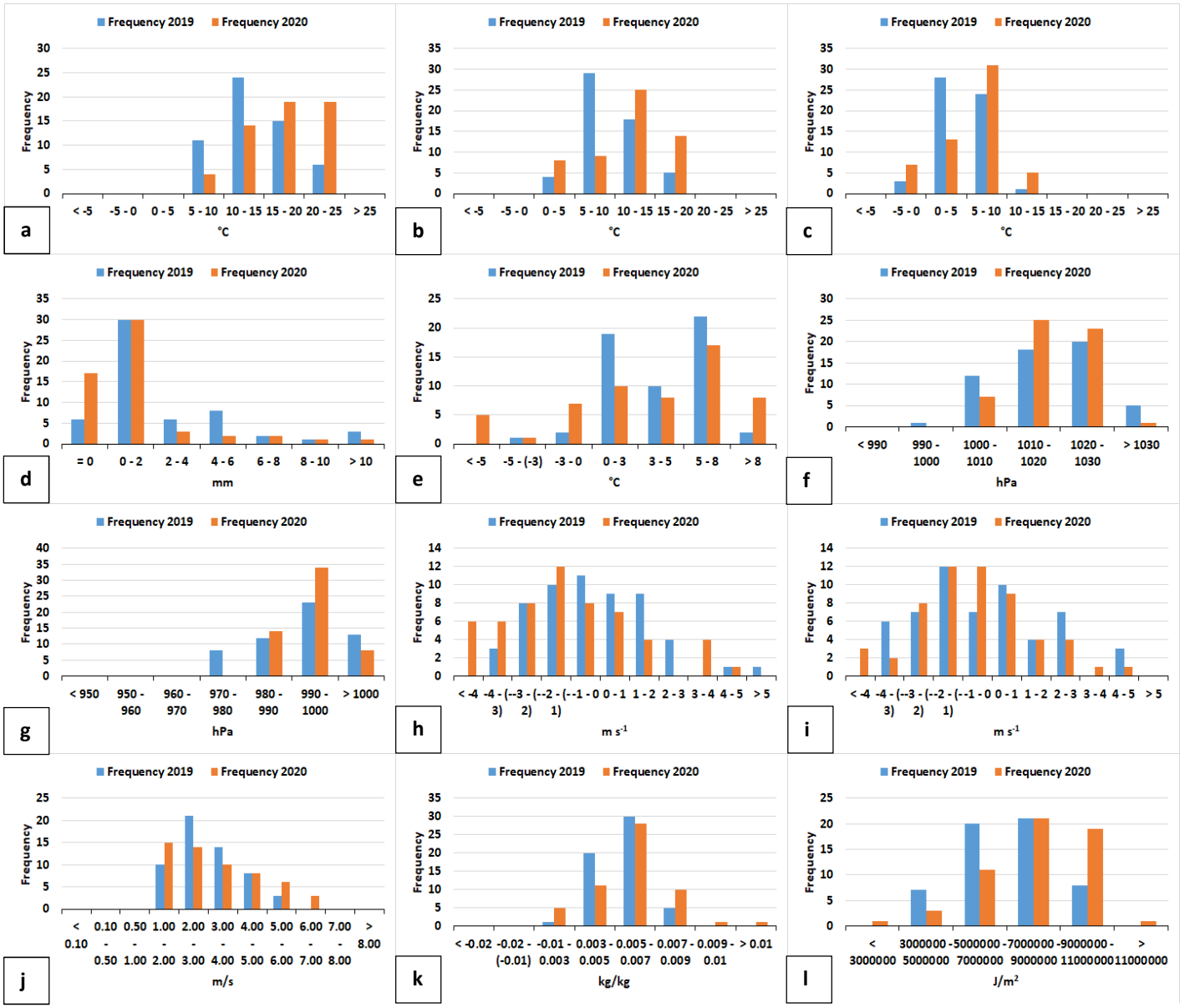

Figure 12. Comparison of the frequencies of 9 meteorological parameters in 2019 and 2020 in the reference period (March 17 - May 11). (**a**) max temperature, (**b**) mean temperature, (**c**) min temperature, (**d**) total precipitation, (**e**) dewpoint, (**f**) mean sea level pressure, (**g**) surface pressure, (**h**) u component of wind, (**i**) v component of wind, (**j**) wind speed, (**k**) humidity, (**l**) solar radiation.

Tabel 2. Chi-square ($\chi 2$) test for homogeneity analysis in all EPCIs of Grand Est. **Df** is the degree of freedom, **p** is the probability of exceeding the critical value, and **CV** is the critical value of the Chi-square distribution. **H0**: homogeneity, the two distributions are equal ($\chi 2$ <= CV); **H1**: difference, the two distributions are unequal ($\chi 2$ > CV).

Entire Grand Est EPCIs					
Parameter	**$\chi 2$**	**df**	**p**	**CV**	**Statement**
Max temperature	13.13	7	0.01	18.4	$\chi 2(7) = 13.13$, $p<.01$, **H0**

Mean temperature	17.26	7	0.01	18.4	$\chi2(7) = 17.26$, p<.01, **H0**
Min temperature	10.65	7	0.01	18.4	$\chi2(7) = 10.65$, p<.01, **H0**
Total precipitation	10.86	6	0.01	16.8	$\chi2(6) = 10.86$, p<.01, **H0**
Dewpoint	15.03	6	0.01	16.8	$\chi2(6) = 15.03$, p<.01, **H0**
Mean sea level	6.33	5	0.01	15.0	$\chi2(5) = 6.33$, p<.01, **H0**
Surface pressure	11.47	6	0.01	16.8	$\chi2(6) = 11.47$, p<.01, **H0**
U component of wind	18.83	10	0.01	23.2	$\chi2(10) = 18.83$, p<.01, **H0**
V component of wind	9.25	10	0.01	23.2	$\chi2(10) = 9.25$, p<.01, **H0**
Wind speed	7.07	10	0.01	23.2	$\chi2(10) = 7.07$, p<.01, **H0**
Humidity	9.02	7	0.01	18.4	$\chi2(7) = 9.02$, p<.01, **H0**
Solar radiation	10.69	5	0.01	15.0	$\chi2(5) = 10.69$, p<.01, **H0**

The decontamination index elaborated in this study and called "Atmospheric Clearance Index" (ACI) is a quantitative measure expressing depollution and permanence of contamination levels taking into account all the pollution parameters entered into the equation. The average value of ACI in the ten urban areas of Grand Est has shown that the greatest depollution during the lockdown has occurred in the cities of Strasbourg, Mulhouse and Colmar. This is also logical not only because the Alsace region is the region with the most economic potential within the Grand Est but also because it is the second region with the highest GDP per capita in France only behind Île-France which is the country's main economic epicenter. As a result, the greatest depollution occurred in urban areas with the highest economic productivity where previously there was also the greatest pollution.

The correlations between ACI and other population and economic development indices show that depollution is a function of the level of economic productivity in an urban area. The strongest correlation is between ACI and population density and this correlation is negative, i.e., inversely proportional. This is because anti-COVID-19 measures affected more the densely populated cities where there have been limitations in the mobility of people and inter-urban transport. Therefore, it is logical that where the population density was higher was the effectiveness of the anti-COVID measures, that is, lower is the value of the ACI that indicates loss of pollution. This also shows that the population density and the activities carried out by it directly affect not only pollution but also decontamination if concrete and effective measures are taken to control urban air quality. The correlations

between ACI and GDP, GVA, number of employees, and active enterprises show that depollution is also an inversely proportional function of the level of economic development of the urban area. Urban areas with higher economic potential were most affected by anti-COVID measures due to indirect constraints on economic activities. Consequently, the cities with the greatest economic potential recorded the highest level of depollution.

Regarding the polynomial curve of degree 2 with which we describe the cloud of points, it should be noted that possibly if a greater number of cities were taken, the points could be described with a linear regression line as well.

6.2. Validation of satellite data with air quality monitoring station data

Every phenomenon observed by means of remote sensing instruments needs to be validated on the ground (Verhoelst et al., 2021). This is mainly due to the effects of the atmosphere that influence the optical satellite data, such as the data from the TROPOMI sensor, which is a DOAS (Differential Optical Absorption Spectrometer) nadir-viewing instrument. The validation data comes from monitoring stations located in urban and peri-urban areas. These data were obtained from the air quality database of the EEA (European Environment Agency) (European Environment Agency (EEA), 2020; European Environment Agnecy (EEA), 2020).

The points in Figure 13 are the monitoring stations where the percentage change was estimated with UTD monitoring data and also using the generalized additive model (GAM). Gridded data were extracted from ECMWFs MARS archive with a 6 hourly resolution (00, 06, 12, 18). Time series for each monitoring station was generated by extracting the ECMWF data for the grid square containing the station. The raster covering the entire area of the Grand Est region was generated using the CAMPS chemical transport modeling estimated for the lockdown conditions (K. L. Chan et al., 2021). Emission reduction factors are estimated during the lockdown period applied to CAMS regional emission inventory and modelled with chemistry-transport models of the regional forecasting service. It is observed

both in the relative difference of the concentration of NO_2 and PM_{10} that the greatest change is concentrated in three urban axes: Reims-Troyes, Metz-Nancy and Strasbourg-Mulhouse.

Figure 14 demonstrate that the ground monitoring data located in the cities is consistent with satellite data (NO_2: R^2=0.37, PM_{10}: R^2=0.62). Technically, where there was the highest concentration of contamination during the reference period in 2019, in 2020 the greater was

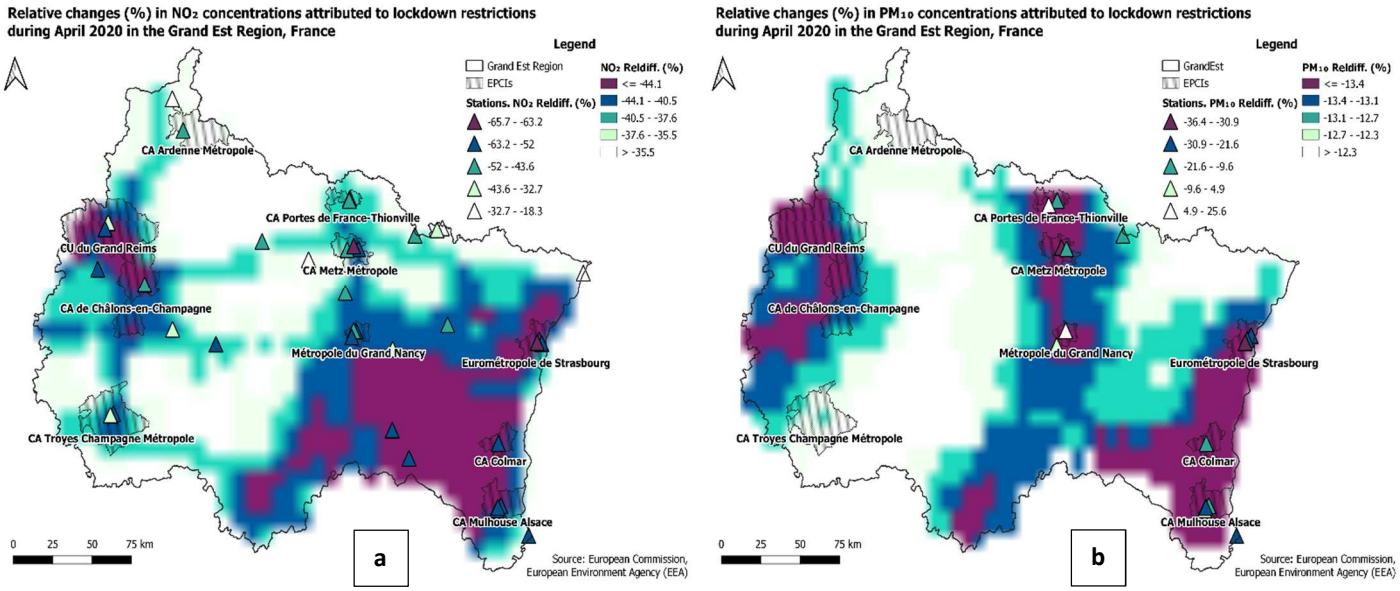

Figure 13. Relative changes (%) in (**a**) NO_2, and (**b**) PM_{10} concentrations attributed to lockdown restrictions during April 2020 in the Grand Est Region, France

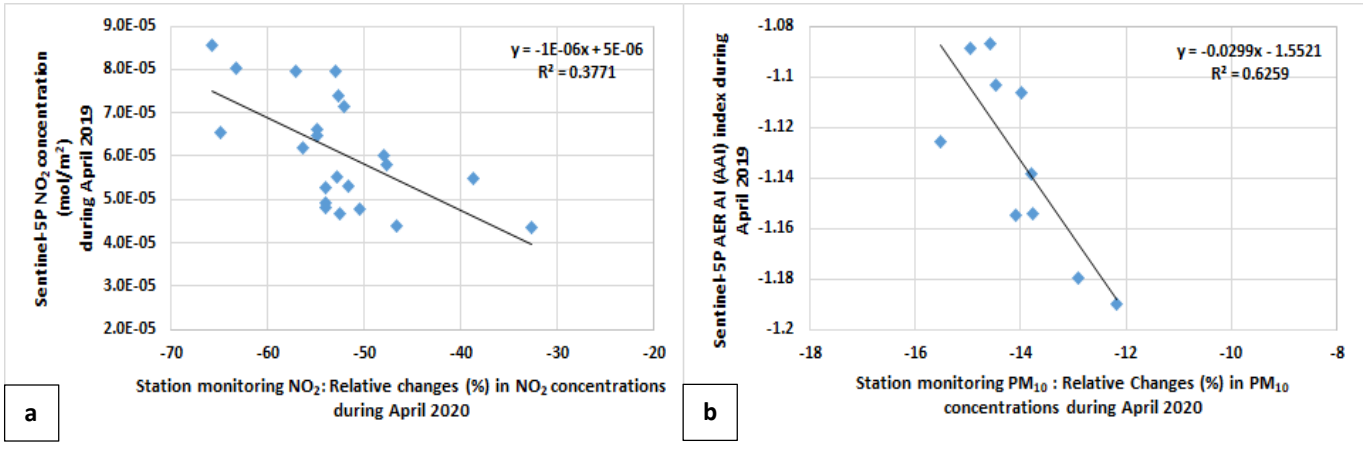

Figure 14. Scatterplots between station monitoring data and satellite data: (**a**) station monitoring NO_2 and Sentinel-5P NO_2, (**b**) station monitoring PM_{10} and Sentinel-5P absorbing aerosol index (AAI)

the change of the percentage reduction.

7. Conclusions

The changes detected in the concentration of the studied air pollutants are based on the elimination of 9 meteorological factors in each of the ten most populated urban areas of Grand Est Region. Analyzing these changes in NO_2 concentration, HCHO, SO_2, O_3, CO, and AAI can be said that air quality in the ten cities and urban areas of Grand Est has been significantly improved during the lockdown in the period 17 March 2020 - 11 May 2020 as a result of the anti-COVID-19 measures. The greatest decline has occurred in the urban areas of Eurométropole de Strasbourg, CA Colmar, CA Mulhouse Alsace. This is explained by the fact that these regions are highly industrialized and, as this important industrial-economic axis is a region bordering the Rhineland-Palatinate industrial region, it also carries out a large amount of commercial and private transport. These sectors of the economy have been the most affected by the cessation due to lockdown, it is, therefore logical that regions with more economic capacity where the air is usually most polluted have experienced the most significant reduction in air pollutants.

The variables that showed the highest average concentration loss compared to 2019 are NO_2 (-33.98%), O_3 (-5.94%), "Absorbing Aerosol Index" (AAI) (-26.82%) and CO (-0.66%). In contrast, the concentration of HCHO and SO_2 has generally increased in the ten urban areas with 13.03% and 47.76%, respectively.

The increase in HCHO and SO_2 concentrations is explained by the following. The main source of HCHO in the atmosphere is the oxidation process of CH_4. In continental regions, the highest oxidation of NMVOCs is emitted mainly by vegetation which results in HCHO increases on a seasonal basis in temperate regions. On the other hand, SO_2 pollution enters the atmosphere mainly due to anthropic activities. The statistics for the Grand Est show an increase in most areas of the smaller cities but the increases are not clearly associated with the cities, but rather a high SO_2 concentration is observed outside the urban areas. In contrast, larger cities like Strasbourg and Reims have had SO_2 declines. This indicates that

the increase in SO_2 comes from sources outside the cities and is not associated directly with COVID-19 affected urban anthropic activities. However, indirectly, the increase in these two gases is an effect of the anti-COVID-19 measures producing an alteration in the distribution of pollutants prior to confinement.

The spatial dimension of atmospheric pollution can exceed the limits of cities and pollution from urban areas can be present on other types of land cover close to the city or conurbation. This has been seen in the case of the ten cities of Grand Est where the reduction of the different types of air pollution often occurred inversely: first greater reduction in the class of land cover closest to the city and then reduction in the urban area. Consequently, the largest air pollution decreases in the medium-sized cities of Grand Est have occurred first around urban areas and then in the built-up urban areas.

The study has shown that the development of a novel depollution index such as the ACI (Atmospheric Clearance Index) can better model the magnitude of the change of the different pollution parameters introduced into the equation because a single quantitative global index can indicate the levels of depollution–pollution permanence. Correlations between ACI index and other population or economic development indices showed that this correlation is negative and statistically significant. This means that depollution caused by anti-COVID measures is a function of population density and other economic factors such as GDP, gross value added, number of employees, and number of active enterprises. In other words, the decontamination produced in the context of the implemented anti-COVID measures depends on the economic potential of an urban region. This has been evidenced by the cases of the cities of Strasbourg, Mulhouse and Colmar in the Alsace region which is the region with the most economic potential in the Grand Est and where there has been the highest level of decontamination.

It can therefore be concluded that the lockdown as an anti-COVID measure have had a beneficial effect on air quality in medium-sized cities in France. On the other hand, it is an

obvious fact that in medium-sized cities also only conscious and regular measures could reduce the concentration of air pollutants and, as a consequence, improve air quality in urban environments.

The policy implications in medium-sized cities should take some concrete steps to reduce air pollution in urban settings. These are summarized below.

- Motor vehicle emissions should be controlled within cities by limiting or prohibiting non-public transport access in centers. In addition, the motor vehicles of public transport should be changed to electric or hybrid and, moreover, the capacity and accessibility of public transport should be increased by introducing more vehicles and making it free of charges for users. This would help, in the long term, to reduce respiratory diseases that cost a lot of treatment for most citizens and cause a high mortality rate.
- Smog causes various problems in many cities such as reduced visibility or respiratory illnesses. Smog could be treated with the increase in green coverage also in medium-sized cities where the approach of such projects does not imply as much financing cost as in larger cities. Trees could be planted in places or squares without vegetation or on the edge of main streets and roads. Planting trees in addition to improving air quality within cities will also serve as a windbreak that prevents dust from moving from one point to another. If more trees can be planted, in the long term, the smog problem will be solved, thus improving the quality of life of the inhabitants.
- City councils must create strict rules and limits for the emissions of toxic substances. Likewise, power plants within a radius of 50 km from cities must ensure that gases emitted into the atmosphere are treated according to European standards to ensure that no harmful substances are emitted into the atmosphere that can reach cities. Such a mechanism is only possible if the environmental

agency monitors compliance with these standards. In the long run, this will mean that toxic gases will be further reduced from our environment and life expectancy will increase due to the reduction of chronic diseases that these toxic gases cause.

Appendice A

Tabel A.1. Results of the homogeneity analysis with chi-square ($\chi 2$) test for the Grand Est EPCIs. **Df** is the degree of freedom, **p** is the probability of exceeding the critical value, and **CV** is the critical value of the Chi-square distribution. **H0**: homogeneity, the two distributions are equal ($\chi 2$ <= CV); **H1**: difference, the two distributions are unequal ($\chi 2$ > CV).

CA Ardenne Métropole					
Parameter	**χ2**	**df**	**p**	**CV**	**Statement**
Max temperature	12.27	7	0.01	18.4	χ2(7) = 12.27, p<.01, H0
Mean temperature	11.41	7	0.01	18.4	χ2(7) = 11.41, p<.01, H0
Minimum temperature	3.90	7	0.01	18.4	χ2(7) = 3.90, p<.01, H0
Total precipitation	12.86	6	0.01	16.8	χ2(6) = 12.86, p<.01, H0
Dewpoint	12.99	6	0.01	16.8	χ2(6) = 12.99, p<.01, H0
Mean sea level pressure	8.66	5	0.01	15.0	χ2(5) = 8.66, p<.01, H0
Surface pressure	11.20	6	0.01	16.8	χ2(6) = 11.20, p<.01, H0
U component of wind	18.84	10	0.01	23.2	χ2(10) = 18.84, p<.01, H0
V component of wind	7.38	10	0.01	23.2	χ2(10) = 7.38, p<.01, H0
Wind speed	11.54	10	0.01	23.2	χ2(10) = 11.54, p<.01, H0
Humidity	10.64	7	0.01	18.4	χ2(7) = 10.64, p<.01, H0
Solar radiation	13.73	5	0.01	15.0	χ2(5) = 13.73, p<.01, H0
CU du Grand Reims					
Parameter	**χ2**	**df**	**p**	**CV**	**Statement**
Max temperature	13.33	7	0.01	18.4	χ2(7) = 13.33, p<.01, H0
Mean temperature	12.07	7	0.01	18.4	χ2(7) = 12.07, p<.01, H0
Minimum temperature	7.51	7	0.01	18.4	χ2(7) = 7.51, p<.01, H0
Total precipitation	14.70	6	0.01	16.8	χ2(6) = 14.70, p<.01, H0
Dewpoint	12.32	6	0.01	16.8	χ2(6) = 12.32, p<.01, H0
Mean sea level pressure	9.61	5	0.01	15.0	χ2(5) = 9.61, p<.01, H0
Surface pressure	4.28	6	0.01	16.8	χ2(6) = 4.28, p<.01, H0
U component of wind	27.94	10	0.01	23.2	χ2(10) = 27.94, p<.01, H1
V component of wind	5.68	10	0.01	23.2	χ2(10) = 5.68, p<.01, H0
Wind speed	8.48	10	0.01	23.2	χ2(10) = 8.48, p<.01, H0
Humidity	9.14	7	0.01	18.4	χ2(7) = 9.14, p<.01, H0
Solar radiation	5.52	5	0.01	15.0	χ2(5) = 5.52, p<.01, H0
CA de Châlons-en-Champagne					
Parameter	**χ2**	**df**	**p**	**CV**	**Statement**
Max temperature	13.99	7	0.01	18.4	χ2(7) = 13.99, p<.01, H0
Mean temperature	11.68	7	0.01	18.4	χ2(7) = 11.68, p<.01, H0
Minimum temperature	8.87	7	0.01	18.4	χ2(7) = 8.87, p<.01, H0
Total precipitation	12.11	6	0.01	16.8	χ2(6) = 12.11, p<.01, H0
Dewpoint	12.58	6	0.01	16.8	χ2(6) = 12.58, p<.01, H0

Mean sea level pressure	6.75	5	0.01	15.0	$\chi2(5) = 6.75$, p<.01, H0
Surface pressure	3.97	6	0.01	16.8	$\chi2(6) = 3.97$, p<.01, H0
U component of wind	19.11	10	0.01	23.2	$\chi2(10) = 19.11$, p<.01, H0
V component of wind	8.53	10	0.01	23.2	$\chi2(10) = 8.53$, p<.01, H0
Wind speed	11.48	10	0.01	23.2	$\chi2(10) = 11.48$, p<.01, H0
Humidity	7.65	7	0.01	18.4	$\chi2(7) = 7.65$, p<.01, H0
Solar radiation	3.22	5	0.01	15.0	$\chi2(5) = 3.22$, p<.01, H0
CA Troyes Champagne Métropole					
Parameter	**χ2**	**df**	**p**	**CV**	**Statement**
Max temperature	14.46	7	0.01	18.4	$\chi2(7) = 14.46$, p<.01, H0
Mean temperature	11.63	7	0.01	18.4	$\chi2(7) = 11.63$, p<.01, H0
Minimum temperature	16.13	7	0.01	18.4	$\chi2(7) = 16.13$, p<.01, H0
Total precipitation	5.82	6	0.01	16.8	$\chi2(6) = 5.82$, p<.01, H0
Dewpoint	19.05	6	0.01	16.8	$\chi2(6) = 19.05$, p<.01, H1
Mean sea level pressure	5.30	5	0.01	15.0	$\chi2(5) = 5.30$, p<.01, H0
Surface pressure	4.97	6	0.01	16.8	$\chi2(6) = 4.97$, p<.01, H0
U component of wind	16.52	10	0.01	23.2	$\chi2(10) = 16.52$, p<.01, H0
V component of wind	7.92	10	0.01	23.2	$\chi2(10) = 7.92$, p<.01, H0
Wind speed	10.04	10	0.01	23.2	$\chi2(10) = 10.04$, p<.01, H0
Humidity	8.95	7	0.01	18.4	$\chi2(7) = 8.95$, p<.01, H0
Solar radiation	12.83	5	0.01	15.0	$\chi2(5) = 12.83$, p<.01, H0
CA Portes de France-Thionville					
Parameter	**χ2**	**df**	**p**	**CV**	**Statement**
Max temperature	8.49	7	0.01	18.4	$\chi2(7) = 8.49$, p<.01, H0
Mean temperature	11.22	7	0.01	18.4	$\chi2(7) = 11.22$, p<.01, H0
Minimum temperature	5.50	7	0.01	18.4	$\chi2(7) = 5.50$, p<.01, H0
Total precipitation	9.07	6	0.01	16.8	$\chi2(6) = 9.07$, p<.01, H0
Dewpoint	11.19	6	0.01	16.8	$\chi2(6) = 11.19$, p<.01, H0
Mean sea level pressure	6.67	5	0.01	15.0	$\chi2(5) = 6.67$, p<.01, H0
Surface pressure	7.52	6	0.01	16.8	$\chi2(6) = 7.52$, p<.01, H0
U component of wind	12.74	10	0.01	23.2	$\chi2(10) = 12.74$, p<.01, H0
V component of wind	4.98	10	0.01	23.2	$\chi2(10) = 4.98$, p<.01, H0
Wind speed	13.82	10	0.01	23.2	$\chi2(10) = 13.82$, p<.01, H0
Humidity	9.02	7	0.01	18.4	$\chi2(7) = 9.02$, p<.01, H0
Solar radiation	12.65	5	0.01	15.0	$\chi2(5) = 12.65$, p<.01, H0
CA Metz Métropole					
Parameter	**χ2**	**df**	**p**	**CV**	**Statement**
Max temperature	11.51	7	0.01	18.4	$\chi2(7) = 11.51$, p<.01, H0
Mean temperature	12.00	7	0.01	18.4	$\chi2(7) = 12.00$, p<.01, H0
Minimum temperature	3.24	7	0.01	18.4	$\chi2(7) = 3.24$, p<.01, H0
Total precipitation	13.96	6	0.01	16.8	$\chi2(6) = 13.96$, p<.01, H0
Dewpoint	10.95	6	0.01	16.8	$\chi2(6) = 10.95$, p<.01, H0
Mean sea level pressure	8.86	5	0.01	15.0	$\chi2(5) = 8.86$, p<.01, H0
Surface pressure	9.11	6	0.01	16.8	$\chi2(6) = 9.11$, p<.01, H0
U component of wind	18.99	10	0.01	23.2	$\chi2(10) = 18.99$, p<.01, H0
V component of wind	5.86	10	0.01	23.2	$\chi2(10) = 5.86$, p<.01, H0
Wind speed	11.69	10	0.01	23.2	$\chi2(10) = 11.69$, p<.01, H0

Humidity	8.93	7	0.01	18.4	$\chi2(7) = 8.93$, p<.01, H0
Solar radiation	12.96	5	0.01	15.0	$\chi2(5) = 12.96$, p<.01, H0
Métropole du Grand Nancy					
Parameter	**χ2**	**df**	**p**	**CV**	**Statement**
Max temperature	16.29	7	0.01	18.4	$\chi2(7) = 16.29$, p<.01, H0
Mean temperature	14.12	7	0.01	18.4	$\chi2(7) = 14.12$, p<.01, H0
Minimum temperature	5.91	7	0.01	18.4	$\chi2(7) = 5.91$, p<.01, H0
Total precipitation	7.54	6	0.01	16.8	$\chi2(6) = 7.54$, p<.01, H0
Dewpoint	14.09	6	0.01	16.8	$\chi2(6) = 14.09$, p<.01, H0
Mean sea level pressure	9.04	5	0.01	15.0	$\chi2(5) = 9.04$, p<.01, H0
Surface pressure	4.75	6	0.01	16.8	$\chi2(6) = 4.75$, p<.01, H0
U component of wind	15.66	10	0.01	23.2	$\chi2(10) = 15.66$, p<.01, H0
V component of wind	21.36	10	0.01	23.2	$\chi2(10) = 21.36$, p<.01, H0
Wind speed	13.04	10	0.01	23.2	$\chi2(10) = 13.04$, p<.01, H0
Humidity	7.84	7	0.01	18.4	$\chi2(7) = 7.84$, p<.01, H0
Solar radiation	12.93	5	0.01	15.0	$\chi2(5) = 12.93$, p<.01, H0
Eurométropole de Strasbourg					
Parameter	**χ2**	**df**	**p**	**CV**	**Statement**
Max temperature	11.97	7	0.01	18.4	$\chi2(7) = 11.97$, p<.01, H0
Mean temperature	16.49	7	0.01	18.4	$\chi2(7) = 16.49$, p<.01, H0
Minimum temperature	15.56	7	0.01	18.4	$\chi2(7) = 15.56$, p<.01, H0
Total precipitation	11.44	6	0.01	16.8	$\chi2(6) = 11.44$, p<.01, H0
Dewpoint	14.35	6	0.01	16.8	$\chi2(6) = 14.35$, p<.01, H0
Mean sea level pressure	5.44	5	0.01	15.0	$\chi2(5) = 5.44$, p<.01, H0
Surface pressure	6.99	6	0.01	16.8	$\chi2(6) = 6.99$, p<.01, H0
U component of wind	15.46	10	0.01	23.2	$\chi2(10) = 15.46$, p<.01, H0
V component of wind	7.74	10	0.01	23.2	$\chi2(10) = 7.74$, p<.01, H0
Wind speed	7.57	10	0.01	23.2	$\chi2(10) = 7.57$, p<.01, H0
Humidity	13.03	7	0.01	18.4	$\chi2(7) = 13.03$, p<.01, H0
Solar radiation	14.13	5	0.01	15.0	$\chi2(5) = 14.13$, p<.01, H0
CA Colmar					
Parameter	**χ2**	**df**	**p**	**CV**	**Statement**
Max temperature	11.85	7	0.01	18.4	$\chi2(7) = 11.85$, p<.01, H0
Mean temperature	16.10	7	0.01	18.4	$\chi2(7) = 16.10$, p<.01, H0
Minimum temperature	11.13	7	0.01	18.4	$\chi2(7) = 11.13$, p<.01, H0
Total precipitation	8.85	6	0.01	16.8	$\chi2(6) = 8.85$, p<.01, H0
Dewpoint	15.51	6	0.01	16.8	$\chi2(6) = 15.51$, p<.01, H0
Mean sea level pressure	8.02	5	0.01	15.0	$\chi2(5) = 8.02$, p<.01, H0
Surface pressure	8.27	6	0.01	16.8	$\chi2(6) = 8.27$, p<.01, H0
U component of wind	12.28	10	0.01	23.2	$\chi2(10) = 12.28$, p<.01, H0
V component of wind	3.95	10	0.01	23.2	$\chi2(10) = 3.95$, p<.01, H0
Wind speed	9.41	10	0.01	23.2	$\chi2(10) = 9.41$, p<.01, H0
Humidity	21.69	7	0.01	18.4	$\chi2(7) = 21.69$, p<.01, H1
Solar radiation	14.96	5	0.01	15.0	$\chi2(5) = 14.96$, p<.01, H0
CA Mulhouse Alsace					
Parameter	**χ2**	**df**	**p**	**CV**	**Statement**
Max temperature	15.82	7	0.01	18.4	$\chi2(7) = 15.82$, p<.01, H0

Mean temperature	16.45	7	0.01	18.4	$\chi2(7) = 16.45$, p<.01, H0
Minimum temperature	8.39	7	0.01	18.4	$\chi2(7) = 8.39$, p<.01, H0
Total precipitation	9.34	6	0.01	16.8	$\chi2(6) = 9.34$, p<.01, H0
Dewpoint	18.43	6	0.01	16.8	$\chi2(6) = 18.43$, p<.01, H1
Mean sea level pressure	7.41	5	0.01	15.0	$\chi2(5) = 7.41$, p<.01, H0
Surface pressure	3.88	6	0.01	16.8	$\chi2(6) = 3.88$, p<.01, H0
U component of wind	11.96	10	0.01	23.2	$\chi2(10) = 11.96$, p<.01, H0
V component of wind	4.86	10	0.01	23.2	$\chi2(10) = 4.86$, p<.01, H0
Wind speed	12.11	10	0.01	23.2	$\chi2(10) = 12.11$, p<.01, H0
Humidity	20.07	7	0.01	18.4	$\chi2(7) = 20.07$, p<.01, H1
Solar radiation	12.21	5	0.01	15.0	$\chi2(5) = 12.21$, p<.01, H0

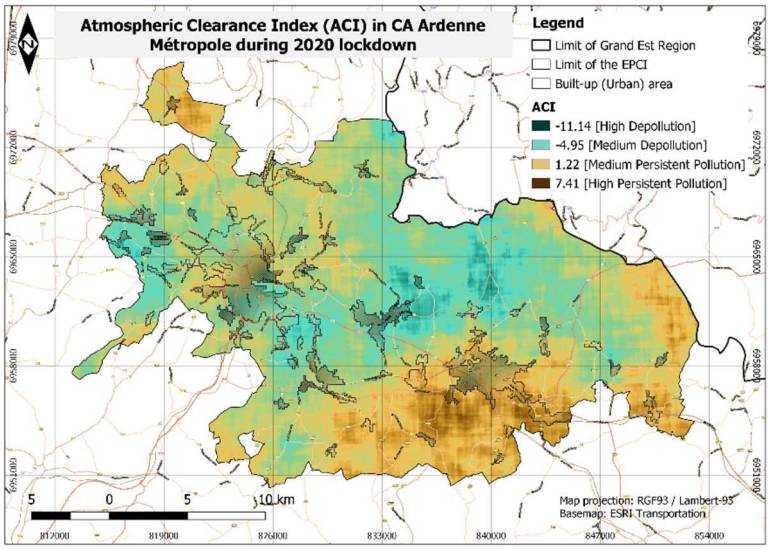

Figure A2. Atmospheric Clearance Index (ACI) in CA Ardenne Métropole during 2020 lockdown

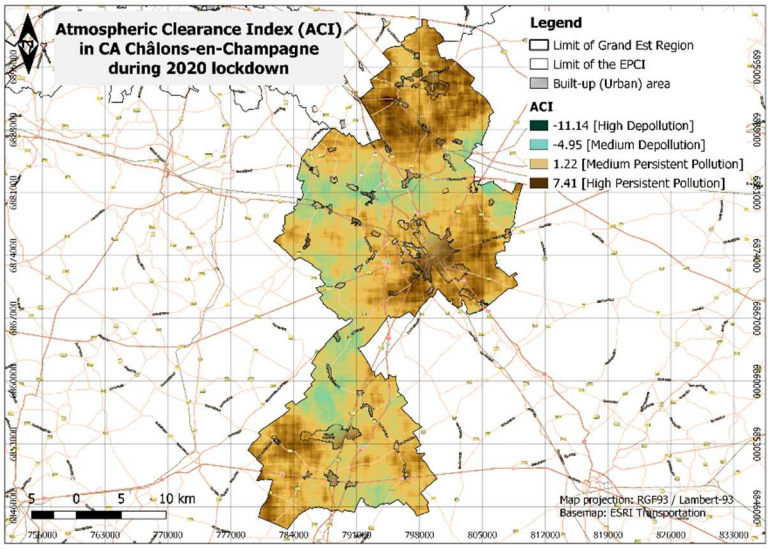

Figure A3. Atmospheric Clearance Index (ACI) in CA Châlons-en-Champagne during 2020 lockdown

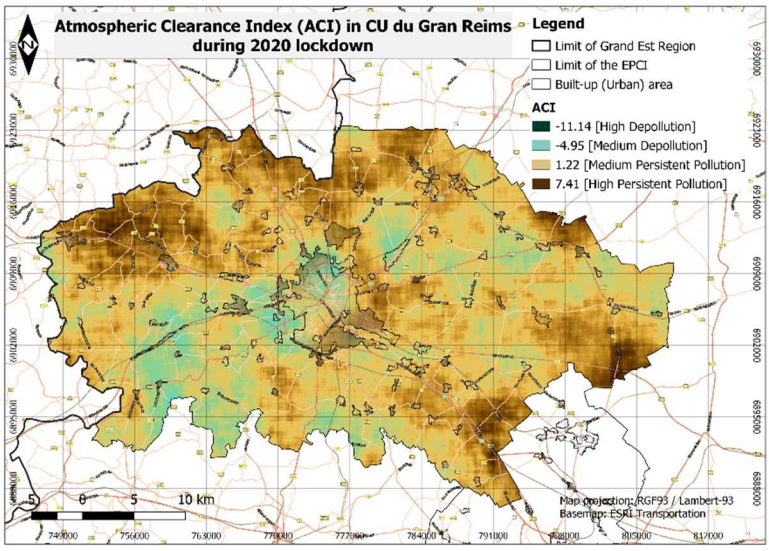

Figure A4. Atmospheric Clearance Index (ACI) in CA du Gran Reims during 2020 lockdown

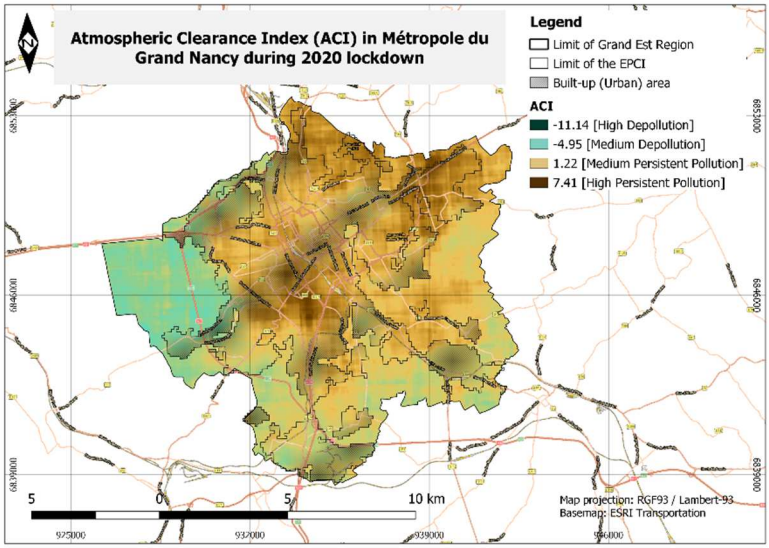

Figure A5. Atmospheric Clearance Index (ACI) in Métropole du Grand Nancy during 2020 lockdown

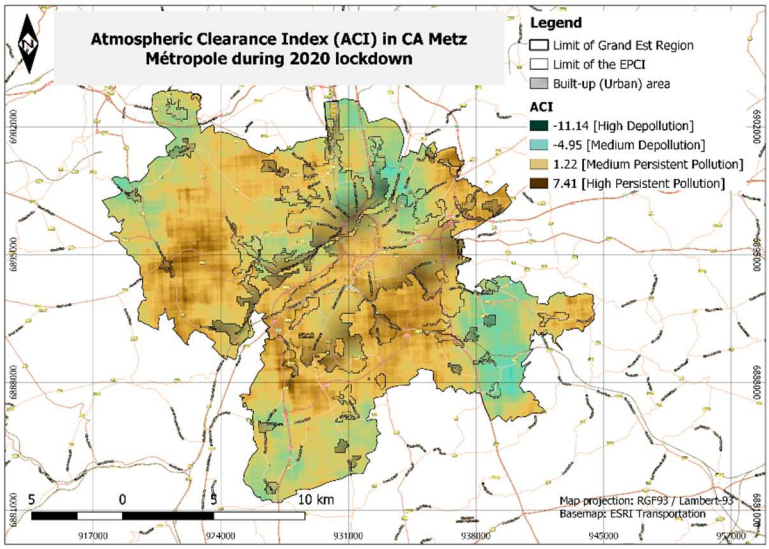

Figure A6. Atmospheric Clearance Index (ACI) in CA Metz Métropole during 2020 lockdown

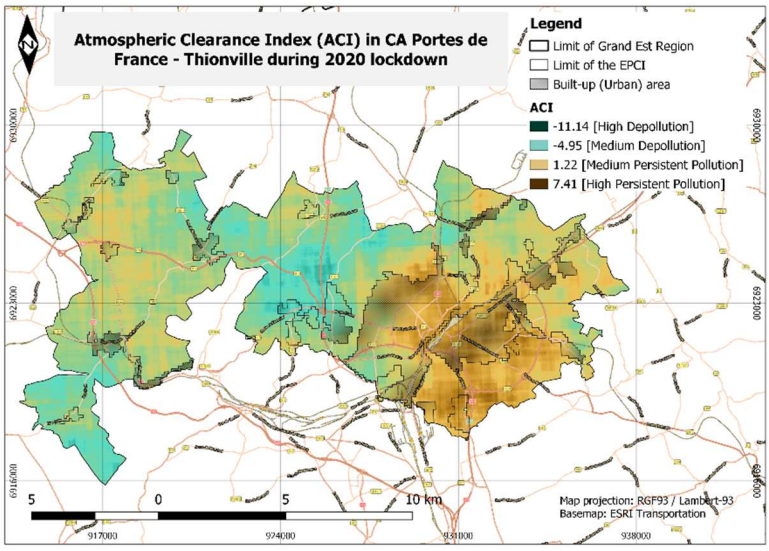

Figure A7. Atmospheric Clearance Index (ACI) in CA Portes de France-Thionville during 2020 lockdown

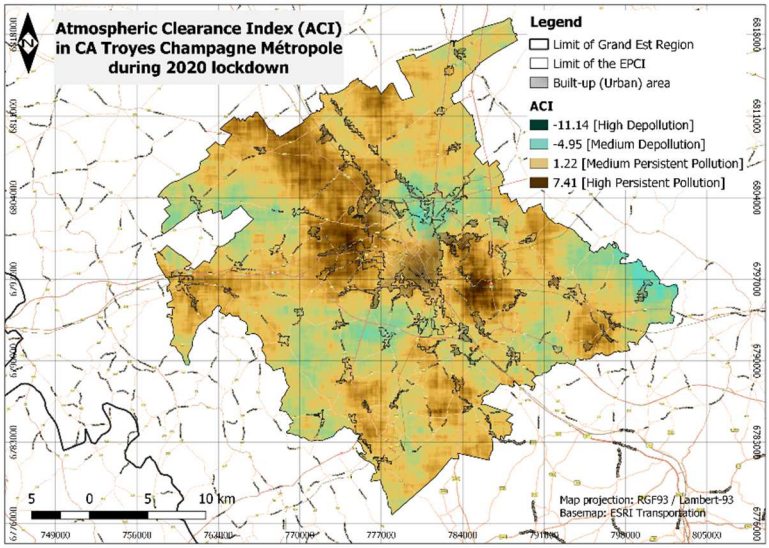

Figure A8. Atmospheric Clearance Index (ACI) in CA Troyes Champagne Métropole during 2020 lockdown

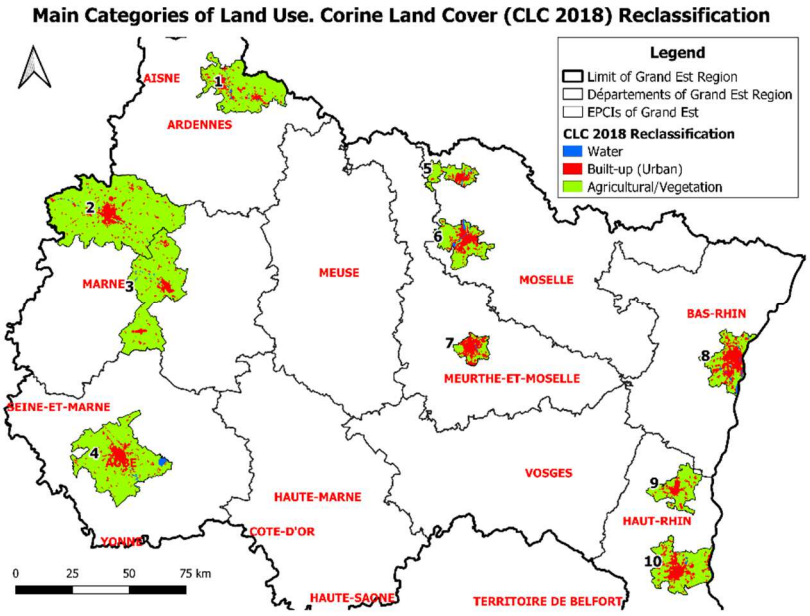

Figure A9. Main Categories of Land Use. Corine Land Cover (CLC 2018) Reclassification

Acknowledgments: The authors would like to thank the free software developers of QGIS and Google Earth Engine for helping our work and also to the European Environment Agency for providing the valuable station monitoring data.

Formatting of funding sources: This research did not receive any grant from funding agencies in the public, commercial, or not-for-profit sectors.

Conflicts of Interest: The authors declare no conflict of interest.

References

Aas, W., Mortier, A., Bowersox, V., Cherian, R., Faluvegi, G., Fagerli, H., Hand, J., Klimont, Z., Galy-Lacaux, C., Lehmann, C. M. B., Myhre, C. L., Myhre, G., Olivié, D., Sato, K., Quaas, J., Rao, P. S. P., Schulz, M., Shindell, D., Skeie, R. B., … Xu, X. (2019). Global and regional trends of atmospheric sulfur. *Scientific Reports*, *9*(1). https://doi.org/10.1038/s41598-018-37304-0

Aggarwal, A., & Toshniwal, D. (2019). Detection of anomalous nitrogen dioxide (NO2) concentration in urban air of India using proximity and clustering methods. *Journal of the Air & Waste Management Association*, *69*(7), 805–822. https://doi.org/10.1080/10962247.2019.1577314

Azimi-Yancheshmeh, R., Moeinaddini, M., Feiznia, S., Riyahi-Bakhtiari, A., Savabieasfahani, M., van Hullebusch, E. D., & Asgari Lajayer, B. (2021). Seasonal and spatial variations in atmospheric PM2.5-bound PAHs in Karaj city, Iran: Sources, distributions, and health risks. *Sustainable Cities and Society*, *72*, 103020. https://doi.org/10.1016/j.scs.2021.103020

Badr, O., & Probert, S. D. (1994). Sources of atmospheric carbon monoxide. *Applied Energy*, *49*(2), 145–195. https://doi.org/10.1016/0306-2619(94)90036-1

Baldasano, J. M. (2020). COVID-19 lockdown effects on air quality by NO2 in the cities of Barcelona and Madrid (Spain). *Science of the Total Environment*, *741*, 140353.

https://doi.org/10.1016/j.scitotenv.2020.140353

Basu, B., Murphy, E., Molter, A., Sarkar Basu, A., Sannigrahi, S., Belmonte, M., & Pilla, F. (2021). Investigating changes in noise pollution due to the COVID-19 lockdown: The case of Dublin, Ireland. *Sustainable Cities and Society*, *65*, 102597. https://doi.org/10.1016/j.scs.2020.102597

Biswas, M. S., Ghude, S. D., Gurnale, D., Prabhakaran, T., & Mahajan, A. S. (2019). Simultaneous Observations of Nitrogen Dioxide, Formaldehyde and Ozone in the Indo-Gangetic Plain. *Aerosol and Air Quality Research*, *19*(8), 1749–1764. https://doi.org/10.4209/aaqr.2018.12.0484

Brenna, H., Kutterolf, S., & Krüger, K. (2019). Global ozone depletion and increase of UV radiation caused by pre-industrial tropical volcanic eruptions. *Scientific Reports*, *9*(1), 1–14. https://doi.org/10.1038/s41598-019-45630-0

Brewer, A. W., Mcelroy, C. T., & Kerr, J. B. (1973). Nitrogen dioxide concentrations in the atmosphere. *Nature*, *246*(5429), 129–133. https://doi.org/10.1038/246129a0

Cadotte, M. (2020). Early evidence that COVID-19 government policies reduce urban air pollution. *EarthArXiv*, 1–9. https://doi.org/10.31223/OSF.IO/NHGJ3

Cameletti, M. (2020). The Effect of Corona Virus Lockdown on Air Pollution: Evidence from the City of Brescia in Lombardia Region (Italy). *Atmospheric Environment*, *239*, 117794. https://doi.org/10.1016/j.atmosenv.2020.117794

Chan, J. F. W., Yuan, S., Kok, K. H., To, K. K. W., Chu, H., Yang, J., Xing, F., Liu, J., Yip, C. C. Y., Poon, R. W. S., Tsoi, H. W., Lo, S. K. F., Chan, K. H., Poon, V. K. M., Chan, W. M., Ip, J. D., Cai, J. P., Cheng, V. C. C., Chen, H., … Yuen, K. Y. (2020). A familial cluster of pneumonia associated with the 2019 novel coronavirus indicating person-to-person transmission: a study of a family cluster. *The Lancet*, *395*(10223), 514–523. https://doi.org/10.1016/S0140-6736(20)30154-9

Chan, K. L., Khorsandi, E., Liu, S., Baier, F., & Valks, P. (2021). Estimation of surface

NO2 concentrations over Germany from TROPOMI satellite observations using a machine learning method. *Remote Sensing*, *13*(5), 1–24. https://doi.org/10.3390/rs13050969

Chatterton, T., Dorling, S., Lovett, A., & Stephenson, M. (2000). Air quality in Norwich, UK multi-scale modelling to assess the significance of city, county and regional pollution sources. *Environmental Monitoring and Assessment*, *65*(1–2), 425–433. https://doi.org/10.1007/978-94-010-0932-4_46

Chen, K., Wang, M., Huang, C., Kinney, P. L., & Anastas, P. T. (2020). Air pollution reduction and mortality benefit during the COVID-19 outbreak in China. In *The Lancet Planetary Health* (Vol. 4, Issue 6, pp. 210–212). Elsevier B.V. https://doi.org/10.1016/S2542-5196(20)30107-8

Chen, Z., Hao, X., Zhang, X., & Chen, F. (2021). Have traffic restrictions improved air quality? A shock from COVID-19. *Journal of Cleaner Production*, *279*, 123622. https://doi.org/10.1016/j.jclepro.2020.123622

Cheng, N., Li, Y., Chen, C., Cheng, B., Sun, F., Wang, B., Li, Q., & Wei, P. (2018). Ground-Level NO2 in Urban Beijing: Trends, Distribution, and Effects of Emission Reduction Measures. *Aerosol and Air Quality Research*, *18*(2), 343–356. https://doi.org/10.4209/aaqr.2017.02.0092

Coccia, M. (2021). Effects of the spread of COVID-19 on public health of polluted cities: results of the first wave for explaining the dejà vu in the second wave of COVID-19 pandemic and epidemics of future vital agents. *Environmental Science and Pollution Research*, 1. https://doi.org/10.1007/s11356-020-11662-7

Conrad, O., Bechtel, B., Bock, M., Dietrich, H., Fischer, E., Gerlitz, L., Wehberg, J., Wichmann, V., & Böhner, J. (2015). System for Automated Geoscientific Analyses (SAGA) v. 2.1.4. *Geoscientific Model Development*, *8*(7), 1991–2007. https://doi.org/10.5194/gmd-8-1991-2015

Conte, L., Szopa, S., Séférian, R., & Bopp, L. (2019). The oceanic cycle of carbon monoxide and its emissions to the atmosphere. *Biogeosciences*, *16*(4), 881–902. https://doi.org/10.5194/bg-16-881-2019

Copernicus Climate Change Service. (n.d.). *ERA5 hourly data on single levels from 1979 to present*. Retrieved July 1, 2021, from https://cds.climate.copernicus.eu/cdsapp#!/dataset/reanalysis-era5-single-levels?tab=overview

Cucinotta, D., & Vanelli, M. (2020). WHO declares COVID-19 a pandemic. In *Acta Biomedica* (Vol. 91, Issue 1, pp. 157–160). Mattioli 1885. https://doi.org/10.23750/abm.v91i1.9397

Dantas, G., Siciliano, B., França, B. B., da Silva, C. M., & Arbilla, G. (2020). The impact of COVID-19 partial lockdown on the air quality of the city of Rio de Janeiro, Brazil. *Science of the Total Environment*, *729*, 139085. https://doi.org/10.1016/j.scitotenv.2020.139085

Darling, D. A., & Robbins, H. (1967). Finding the Size of a Finite Population on JSTOR. *The Annals of Mathematical Statistics*, *38*(5), 1392–1398. https://www.jstor.org/stable/2238956?refreqid=excelsior%3A40721dc15b9f4fa322538c304f2d81bd&seq=1

Dutheil, F., Baker, J. S., & Navel, V. (2020). COVID-19 as a factor influencing air pollution? In *Environmental Pollution* (Vol. 263). Elsevier Ltd. https://doi.org/10.1016/j.envpol.2020.114466

Earth Engine Data Catalog. (n.d.-a). *ERA5-Land hourly - ECMWF climate reanalysis*. Retrieved July 1, 2021, from https://developers.google.com/earth-engine/datasets/catalog/ECMWF_ERA5_LAND_HOURLY

Earth Engine Data Catalog. (n.d.-b). *ERA5 Daily aggregates - Latest climate reanalysis produced by ECMWF / Copernicus Climate Change Service*. Retrieved July 1, 2021,

from https://developers.google.com/earth-engine/datasets/catalog/ECMWF_ERA5_DAILY

Earth Engine Data Catalog. (n.d.-c). *GLDAS-2.1: Global Land Data Assimilation System*. Retrieved July 1, 2021, from https://developers.google.com/earth-engine/datasets/catalog/NASA_GLDAS_V021_NOAH_G025_T3H

ESA - Copernicus. (n.d.-a). *Climate Data Store*. Retrieved July 1, 2021, from https://cds.climate.copernicus.eu/cdsapp#!/home

ESA - Copernicus. (n.d.-b). *Sentinel-5P Datasets in Earth Engine | Earth Engine Data Catalog*. Retrieved March 30, 2021, from https://developers.google.com/earth-engine/datasets/catalog/sentinel-5p

European Comission. (2017). *Special Eurobarometer 468: Attitudes of European citizens towards the environment - Datasets*. https://data.europa.eu/euodp/en/data/dataset/S2156_88_1_468_ENG

European Environment Agency (EEA). (2020, October 26). *Relative changes (%) in PM10 concentrations attributed to lockdown restrictions during April 2020 — European Environment Agency*. https://www.eea.europa.eu/data-and-maps/figures/relative-changes-in-pm10-concentrations

European Environment Agnecy (EEA). (2020, October 26). *Relative changes (%) in NO2 concentrations attributed to lockdown restrictions during April 2020 — European Environment Agency*. https://www.eea.europa.eu/data-and-maps/figures/relative-changes-in-no2-concentrations

Eurostat. (n.d.). *Database - Regions - Eurostat*. Retrieved July 1, 2021, from https://ec.europa.eu/eurostat/web/regions/data/database

Fattorini, D., & Regoli, F. (2020). Role of the chronic air pollution levels in the Covid-19 outbreak risk in Italy. In *Environmental Pollution* (Vol. 264). Elsevier Ltd. https://doi.org/10.1016/j.envpol.2020.114732

Filonchyk, M., Hurynovich, V., & Yan, H. (2020). Impact of Covid-19 lockdown on air quality in the Poland, Eastern Europe. *Environmental Research*. https://doi.org/10.1016/j.envres.2020.110454

Galeazzi, A., Cinelli, M., Bonaccorsi, G., Pierri, F., Schmidt, A. L., Scala, A., Pammolli, F., & Quattrociocchi, W. (2020). Human Mobility in Response to COVID-19 in France, Italy and UK. *ArXiv*. http://arxiv.org/abs/2005.06341

Gama, C., Relvas, H., Lopes, M., & Monteiro, A. (2021). The impact of COVID-19 on air quality levels in Portugal: A way to assess traffic contribution. *Environmental Research*, *193*. https://doi.org/10.1016/j.envres.2020.110515

Go, S., Kim, M., Kim, J., Park, S., Jeong, U., & Choi, M. (2017). Detection of Absorbing Aerosol Using Single Near-UV Radiance Measurements from a Cloud and Aerosol Imager. *Remote Sensing*, *9*(4), 378. https://doi.org/10.3390/rs9040378

Hammer, M. S., Martin, R. V., Van Donkelaar, A., Buchard, V., Torres, O., Ridley, D. A., & Spurr, R. J. D. (2016). Interpreting the ultraviolet aerosol index observed with the OMI satellite instrument to understand absorption by organic aerosols: Implications for atmospheric oxidation and direct radiative effects. *Atmospheric Chemistry and Physics*, *16*(4), 2507–2523. https://doi.org/10.5194/acp-16-2507-2016

Higham, J. E., Ramírez, C. A., Green, M. A., & Morse, A. P. (2021). UK COVID-19 lockdown: 100 days of air pollution reduction? *Air Quality, Atmosphere and Health*, *14*(3), 325–332. https://doi.org/10.1007/s11869-020-00937-0

Huang, C., Wang, Y., Li, X., Ren, L., Zhao, J., Hu, Y., Zhang, L., Fan, G., Xu, J., Gu, X., Cheng, Z., Yu, T., Xia, J., Wei, Y., Wu, W., Xie, X., Yin, W., Li, H., Liu, M., … Cao, B. (2020). Clinical features of patients infected with 2019 novel coronavirus in Wuhan, China. *The Lancet*, *395*(10223), 497–506. https://doi.org/10.1016/S0140-6736(20)30183-5

Ikhlasse, H., Benjamin, D., Vincent, C., & Hicham, M. (2021). Environmental impacts of

pre/during and post-lockdown periods on prominent air pollutants in France. *Environment, Development and Sustainability*, 1–22. https://doi.org/10.1007/s10668-021-01241-2

Javed, Z., Wang, Y., Xie, M., Tanvir, A., Rehman, A., Ji, X., Xing, C., Shakoor, A., & Liu, C. (2020). Investigating the impacts of the COVID-19 lockdown on trace gases using ground-based MAX-DOAS observations in Nanjing, China. *Remote Sensing*, *12*(23), 1–17. https://doi.org/10.3390/rs12233939

Kerimray, A., Baimatova, N., Ibragimova, O. P., Bukenov, B., Kenessov, B., Plotitsyn, P., & Karaca, F. (2020). Assessing air quality changes in large cities during COVID-19 lockdowns: The impacts of traffic-free urban conditions in Almaty, Kazakhstan. *Science of the Total Environment*, *730*, 139179. https://doi.org/10.1016/j.scitotenv.2020.139179

Kim, E., & Hopke, P. K. (2008). Source characterization of ambient fine particles at multiple sites in the Seattle area. *Atmospheric Environment*, *42*(24), 6047–6056. https://doi.org/10.1016/j.atmosenv.2008.03.032

Kovács, K. D. (2021a). *Retrieving climate data from ECMWF_ERA5_DAILY: Grand Est Urban Areas - Earth Engine Code Editor*. Google Earth Engine. https://code.earthengine.google.com/c8e51091665cc4eb409b69614bac5ffc

Kovács, K. D. (2021b). *Retrieving climate data from ECMWF_ERA5_LAND_HOURLY: Grand Est Urban Areas - Earth Engine Code Editor*. Google Earth Engine. https://code.earthengine.google.com/8c65acb73c7850625a1e06960c082d9f

Kovács, K. D. (2021c). *Retrieving climate data from NASA_GLDAS_V021_NOAH_G025_T3H: Grand Est Urban Areas - Earth Engine Code Editor*. Google Earth Engine. https://code.earthengine.google.com/7f9d0346778cab602e3d31eb5dabbc5f

Kovács, K. D. (2021d). *S5P Atmospheric Analysis: Grand Est Urban Areas - Earth Engine*

Code Editor. Google Earth Engine. https://code.earthengine.google.com/4c954af1eee7b8abf8ae7798e61dffc1

Kumar, P., Hama, S., Omidvarborna, H., Sharma, A., Sahani, J., Abhijith, K. V., Debele, S. E., Zavala-Reyes, J. C., Barwise, Y., & Tiwari, A. (2020). Temporary reduction in fine particulate matter due to 'anthropogenic emissions switch-off' during COVID-19 lockdown in Indian cities. *Sustainable Cities and Society*, *62*, 102382. https://doi.org/10.1016/j.scs.2020.102382

Kumari, P., & Toshniwal, D. (2020). Impact of lockdown on air quality over major cities across the globe during COVID-19 pandemic. *Urban Climate*, *34*, 100719. https://doi.org/10.1016/j.uclim.2020.100719

Lee, Y.-Y., Wang, L.-C., Zhu, J., Wu, J.-L., & Lee, K.-L. (2018). Atmospheric PM2.5 and Polychlorinated Dibenzo-p-dioxins and Dibenzofurans in Taiwan. *Aerosol and Air Quality Research*, *18*(3), 762–779. https://doi.org/10.4209/aaqr.2018.02.0050

Liang, D., Wang, Y.-Q., Ma, C., & Wang, Y.-J. (2017). Variability in Transport Pathways and Source Areas of PM10 in Beijing during 2009–2012. *Aerosol and Air Quality Research*, *16*(12), 3130–3141. https://doi.org/10.4209/aaqr.2016.02.0090

Loey, M., Manogaran, G., Taha, M. H. N., & Khalifa, N. E. M. (2021). Fighting against COVID-19: A novel deep learning model based on YOLO-v2 with ResNet-50 for medical face mask detection. *Sustainable Cities and Society*, *65*, 102600. https://doi.org/10.1016/j.scs.2020.102600

Lozhkina, O., Lozhkin, V., Nevmerzhitsky, N., Tarkhov, D., & Vasilyev, A. (2016). Motor transport related harmful PM2.5 and PM10: From onroad measurements to the modelling of air pollution by neural network approach on street and urban level. *Journal of Physics: Conference Series*, *772*(1), 012031. https://doi.org/10.1088/1742-6596/772/1/012031

Luecken, D. J., Hutzell, W. T., Strum, M. L., & Pouliot, G. A. (2012). Regional sources of

atmospheric formaldehyde and acetaldehyde, and implications for atmospheric modeling. *Atmospheric Environment*, *47*, 477–490. https://doi.org/10.1016/j.atmosenv.2011.10.005

Luecken, D. J., Napelenok, S. L., Strum, M., Scheffe, R., & Phillips, S. (2018). Sensitivity of Ambient Atmospheric Formaldehyde and Ozone to Precursor Species and Source Types Across the United States. *Environmental Science and Technology*, *52*(8), 4668–4675. https://doi.org/10.1021/acs.est.7b05509

Magazzino, C., Mele, M., & Sarkodie, S. A. (2021). The nexus between COVID-19 deaths, air pollution and economic growth in New York state: Evidence from Deep Machine Learning. *Journal of Environmental Management*, *286*, 112241. https://doi.org/10.1016/j.jenvman.2021.112241

Magazzino, C., Mele, M., & Schneider, N. (2020). The relationship between air pollution and COVID-19-related deaths: An application to three French cities. *Applied Energy*, *279*, 115835. https://doi.org/10.1016/j.apenergy.2020.115835

Martelletti, L., & Martelletti, P. (2020). Air Pollution and the Novel Covid-19 Disease: a Putative Disease Risk Factor. *SN Comprehensive Clinical Medicine*, *2*(4), 383–387. https://doi.org/10.1007/s42399-020-00274-4

Matawle, J. L., Pervez, S., Dewangan, S., Shrivastava, A., Tiwari, S., Pant, P., Deb, M. K., & Pervez, Y. (2015). Characterization of PM2.5 Source Profiles for Traffic and Dust Sources in Raipur, India. *Aerosol and Air Quality Research*, *15*(7), 2537–2548. https://doi.org/10.4209/aaqr.2015.04.0222

Matus, K., Nam, K. M., Selin, N. E., Lamsal, L. N., Reilly, J. M., & Paltsev, S. (2012). Health damages from air pollution in China. *Global Environmental Change*, *22*(1), 55–66. https://doi.org/10.1016/j.gloenvcha.2011.08.006

Mele, M., & Magazzino, C. (2021). Pollution, economic growth, and COVID-19 deaths in India: a machine learning evidence. *Environmental Science and Pollution Research*,

28(3), 2669–2677. https://doi.org/10.1007/s11356-020-10689-0

Meng, F., Wang, J., Li, T., & Fang, C. (2020). Pollution characteristics, transport pathways, and potential source regions of pm2.5 and pm10 in changchun city in 2018. *International Journal of Environmental Research and Public Health*, *17*(18), 1–19. https://doi.org/10.3390/ijerph17186585

Menut, L., Bessagnet, B., Siour, G., Mailler, S., Pennel, R., & Cholakian, A. (2020). Impact of lockdown measures to combat Covid-19 on air quality over western Europe. *Science of the Total Environment*, *741*, 140426. https://doi.org/10.1016/j.scitotenv.2020.140426

Monks, P. S., Archibald, A. T., Colette, A., Cooper, O., Coyle, M., Derwent, R., Fowler, D., Granier, C., Law, K. S., Mills, G. E., Stevenson, D. S., Tarasova, O., Thouret, V., Von Schneidemesser, E., Sommariva, R., Wild, O., & Williams, M. L. (2015). Tropospheric ozone and its precursors from the urban to the global scale from air quality to short-lived climate forcer. In *Atmospheric Chemistry and Physics* (Vol. 15, Issue 15, pp. 8889–8973). Copernicus GmbH. https://doi.org/10.5194/acp-15-8889-2015

Muhammad, S., Long, X., & Salman, M. (2020). COVID-19 pandemic and environmental pollution: A blessing in disguise? *Science of the Total Environment*, *728*. https://doi.org/10.1016/j.scitotenv.2020.138820

Munir, S., Coskuner, G., Jassim, M. S., Aina, Y. A., Ali, A., & Mayfield, M. (2021). Changes in Air Quality Associated with Mobility Trends and Meteorological Conditions during COVID-19 Lockdown in Northern England, UK. *Atmosphere*, *12*(4), 504. https://doi.org/10.3390/atmos12040504

Nakada, L. Y. K., & Urban, R. C. (2020). COVID-19 pandemic: Impacts on the air quality during the partial lockdown in São Paulo state, Brazil. *Science of the Total Environment*, *730*, 139087. https://doi.org/10.1016/j.scitotenv.2020.139087

NASA GES DISC at NASA Goddard Space Flight Center. (n.d.). *GES DISC Dataset:*

GLDAS Noah Land Surface Model L4 3 hourly 0.25 x 0.25 degree V2.1 (GLDAS_NOAH025_3H 2.1). Retrieved July 1, 2021, from https://disc.gsfc.nasa.gov/datasets/GLDAS_NOAH025_3H_2.1/summary

Nguyen, T. P. M., Bui, T. H., Nguyen, M. K., Nguyen, T. H., Vu, V. T., & Pham, H. L. (2021). Impact of Covid-19 partial lockdown on PM2.5, SO2, NO2, O3, and trace elements in PM2.5 in Hanoi, Vietnam. *Environmental Science and Pollution Research*, 1. https://doi.org/10.1007/s11356-021-13792-y

Ogen, Y. (2020). Assessing nitrogen dioxide (NO2) levels as a contributing factor to coronavirus (COVID-19) fatality. *Science of the Total Environment*. https://doi.org/10.1016/j.scitotenv.2020.138605

Peel, J. L., Haeuber, R., Garcia, V., Russell, A. G., & Neas, L. (2013). Impact of nitrogen and climate change interactions on ambient air pollution and human health. *Biogeochemistry*, *114*(1–3), 121–134. https://doi.org/10.1007/s10533-012-9782-4

Piazzola, J., Bruch, W., Desnues, C., Parent, P., Yohia, C., & Canepa, E. (2021). Influence of Meteorological Conditions and Aerosol Properties on the COVID-19 Contamination of the Population in Coastal and Continental Areas in France: Study of Offshore and Onshore Winds. *Atmosphere*, *12*(4), 523. https://doi.org/10.3390/atmos12040523

Robbins, R. C., Borg, K. M., & Robinson, E. (1968). Carbon monoxide in the atmosphere. *Journal of the Air Pollution Control Association*, *18*(2), 106–110. https://doi.org/10.1080/00022470.1968.10469094

Rugani, B., & Caro, D. (2020). Impact of COVID-19 outbreak measures of lockdown on the Italian Carbon Footprint. *Science of the Total Environment*, *737*, 139806. https://doi.org/10.1016/j.scitotenv.2020.139806

Saito, S., Nagao, I., & Tanaka, H. (2002). Relationship of NOX and NMHC to photochemical O3 production in a coastal and metropolitan areas of Japan. *Atmospheric Environment*, *36*(8), 1277–1286. https://doi.org/10.1016/S1352-

2310(01)00557-X

Sbai, S. E., Mejjad, N., Norelyaqine, A., & Bentayeb, F. (2021). Air quality change during the COVID-19 pandemic lockdown over the Auvergne-Rhône-Alpes region, France. *Air Quality, Atmosphere and Health*, 1–12. https://doi.org/10.1007/s11869-020-00965-w

Schauer, J. J., Rogge, W. F., Hildemann, L. M., Mazurek, M. A., Cass, G. R., & Simoneit, B. R. T. (1996). Source apportionment of airborne particulate matter using organic compounds as tracers. *Atmospheric Environment*, *30*(22), 3837–3855. https://doi.org/10.1016/1352-2310(96)00085-4

Sharma, S., Zhang, M., Anshika, Gao, J., Zhang, H., & Kota, S. H. (2020). Effect of restricted emissions during COVID-19 on air quality in India. *Science of the Total Environment*, *728*, 138878. https://doi.org/10.1016/j.scitotenv.2020.138878

She, Q., Peng, X., Xu, Q., Long, L., Wei, N., Liu, M., Han, J., Xiang, W., Peng, X., Jia, W., & Zhou, T. (2017). Air quality and its response to satellite-derived urban form in the Yangtze River Delta, China. *Ecological Indicators*, *75*, 297–306. https://doi.org/10.1016/j.ecolind.2016.12.045

Shen, F., Ge, X., Hu, J., Nie, D., Tian, L., & Chen, M. (2017). Air pollution characteristics and health risks in Henan Province, China. *Environmental Research*, *156*, 625–634. https://doi.org/10.1016/j.envres.2017.04.026

Shi, X., & Brasseur, G. P. (2020). The Response in Air Quality to the Reduction of Chinese Economic Activities During the COVID-19 Outbreak. *Geophysical Research Letters*, *47*(11), e2020GL088070. https://doi.org/10.1029/2020GL088070

Skirienė, A. F., & Stasiškienė, Ž. (2021). COVID-19 and Air Pollution: Measuring Pandemic Impact to Air Quality in Five European Countries. *Atmosphere*, *12*(3), 290. https://doi.org/10.3390/atmos12030290

Song, Y., Tang, X., Xie, S., Zhang, Y., Wei, Y., Zhang, M., Zeng, L., & Lu, S. (2007).

Source apportionment of PM2.5 in Beijing in 2004. *Journal of Hazardous Materials*, *146*(1–2), 124–130. https://doi.org/10.1016/j.jhazmat.2006.11.058

Su, Z., Duan, Z., Deng, B., Liu, Y., & Chen, X. (2021). Impact of the COVID-19 Lockdown on Air Quality Trends in Guiyang, Southwestern China. *Atmosphere*, *12*(4), 422. https://doi.org/10.3390/atmos12040422

Tao, J., Ho, K. F., Chen, L., Zhu, L., Han, J., & Xu, Z. (2009). Effect of chemical composition of PM2.5 on visibility in Guangzhou, China, 2007 spring. *Particuology*, *7*(1), 68–75. https://doi.org/10.1016/j.partic.2008.11.002

Tian, H., Liu, Y., Li, Y., Wu, C. H., Chen, B., Kraemer, M. U. G., Li, B., Cai, J., Xu, B., Yang, Q., Wang, B., Yang, P., Cui, Y., Song, Y., Zheng, P., Wang, Q., Bjornstad, O. N., Yang, R., Grenfell, B. T., … Dye, C. (2020). An investigation of transmission control measures during the first 50 days of the COVID-19 epidemic in China. *Science*, *368*(6491), 638–642. https://doi.org/10.1126/science.abb6105

Tian, X., An, C., Chen, Z., & Tian, Z. (2021). Assessing the impact of COVID-19 pandemic on urban transportation and air quality in Canada. *Science of the Total Environment*, *765*, 144270. https://doi.org/10.1016/j.scitotenv.2020.144270

Tsatsakis, A., Petrakis, D., Nikolouzakis, T. K., Docea, A. O., Calina, D., Vinceti, M., Goumenou, M., Kostoff, R. N., Mamoulakis, C., Aschner, M., & Hernández, A. F. (2020). COVID-19, an opportunity to reevaluate the correlation between long-term effects of anthropogenic pollutants on viral epidemic/pandemic events and prevalence. *Food and Chemical Toxicology*, *141*, 111418. https://doi.org/10.1016/j.fct.2020.111418

Turner, M. C., Jerrett, M., Pope, C. A., Krewski, D., Gapstur, S. M., Diver, W. R., Beckerman, B. S., Marshall, J. D., Su, J., Crouse, D. L., & Burnett, R. T. (2016). Long-Term Ozone Exposure and Mortality in a Large Prospective Study. *American Journal of Respiratory and Critical Care Medicine*, *193*(10), 1134–1142.

https://doi.org/10.1164/rccm.201508-1633OC

United States Environmental Protection Agency. (2019). *Sulfur Dioxide Basics | Sulfur Dioxide (SO2) Pollution | US EPA*. https://www.epa.gov/so2-pollution/sulfur-dioxide-basics

Verhoelst, T., Compernolle, S., Pinardi, G., Lambert, J. C., Eskes, H. J., Eichmann, K. U., Fjæraa, A. M., Granville, J., Niemeijer, S., Cede, A., Tiefengraber, M., Hendrick, F., Pazmiño, A., Bais, A., Bazureau, A., Folkert Boersma, K., Bognar, K., Dehn, A., Donner, S., … Zehner, C. (2021). Ground-based validation of the Copernicus Sentinel-5P TROPOMI NO2 measurements with the NDACC ZSL-DOAS, MAX-DOAS and Pandonia global networks. *Atmospheric Measurement Techniques*, *14*(1), 481–510. https://doi.org/10.5194/amt-14-481-2021

Vie Publique. (n.d.-a). *La coopération intercommunale et les EPCI| Vie publique.fr*. Retrieved March 30, 2021, from https://www.vie-publique.fr/fiches/20118-la-cooperation-intercommunale-et-les-epci

Vie Publique. (n.d.-b). *Les mécanismes de fonctionnement des EPCI| Vie publique.fr*. Retrieved March 30, 2021, from https://www.vie-publique.fr/fiches/20119-les-mecanismes-de-fonctionnement-des-epci

Wang, H., Xu, J., Zhang, M., Yang, Y., Shen, X., Wang, Y., Chen, D., & Guo, J. (2014). A study of the meteorological causes of a prolonged and severe haze episode in January 2013 over central-eastern China. *Atmospheric Environment*, *98*, 146–157. https://doi.org/10.1016/j.atmosenv.2014.08.053

Wang, Q., & Li, S. (2021). Nonlinear impact of COVID-19 on pollutions – Evidence from Wuhan, New York, Milan, Madrid, Bandra, London, Tokyo and Mexico City. *Sustainable Cities and Society*, *65*, 102629. https://doi.org/10.1016/j.scs.2020.102629

Wang, W., Cui, K., Zhao, R., Hsieh, L.-T., & Lee, W.-J. (2018). Characterization of the Air Quality Index for Wuhu and Bengbu Cities, China. *Aerosol and Air Quality Research*,

18(5), 1198–1220. https://doi.org/10.4209/aaqr.2018.04.0135

Wang, Z., Zheng, F., Zhang, W., & Wang, S. (2018). Analysis of SO2 Pollution Changes of Beijing-Tianjin-Hebei Region over China Based on OMI Observations from 2006 to 2017. *Advances in Meteorology*, *2018*. https://doi.org/10.1155/2018/8746068

Wei, X., Chang, N. Bin, Bai, K., & Gao, W. (2020). Satellite remote sensing of aerosol optical depth: advances, challenges, and perspectives. *Critical Reviews in Environmental Science and Technology*, *50*(16), 1640–1725. https://doi.org/10.1080/10643389.2019.1665944

WHO. (2020a). *Updated WHO advice for international traffic in relation to the outbreak of the novel coronavirus 2019-nCoV*. https://www.who.int/news-room/articles-detail/updated-who-advice-for-international-traffic-in-relation-to-the-outbreak-of-the-novel-coronavirus-2019-ncov

WHO. (2020b). *Updated WHO recommendations for international traffic in relation to COVID-19 outbreak*. https://www.who.int/news-room/articles-detail/updated-who-recommendations-for-international-traffic-in-relation-to-covid-19-outbreak

WHO. (2020c). *Weekly epidemiological update - 15 December 2020*. https://www.who.int/publications/m/item/weekly-epidemiological-update---15-december-2020

WHO. (2020d). *World Health Organization. Nowel Coronavirus (19-nCoV) Situation Report—1. 21 January 2020.* https://www.who.int/docs/default-source/coronaviruse/situation-reports/20200121-sitrep-1-2019-ncov.pdf

Wu, S.-P., Xu, C., Dai, L.-H., Zhang, N., Wei, Y., Gao, Y., Yan, J.-P., & Schwab, J. J. (2019). Source Apportionment of PM2.5 at Urban and Suburban Sites in a Port City of Southeastern China. *Aerosol and Air Quality Research*, *19*(9), 2017–2031. https://doi.org/10.4209/aaqr.2019.01.0007

Wu, Y., Lu, B., Zhu, X., Wang, A., Yang, M., Gu, S., Wang, X., Leng, P., Zierold, K. M.,

Li, X., Tang, K. K., Fang, L., Huang, R., Xu, G., & Chen, L. (2019). Seasonal Variations, Source Apportionment, and Health Risk Assessment of Heavy Metals in PM2.5 in Ningbo, China. *Aerosol and Air Quality Research*, *19*(9), 2083–2092. https://doi.org/10.4209/aaqr.2018.12.0452

Xu, G., Jiao, L., Zhang, B., Zhao, S., Yuan, M., Gu, Y., Liu, J., & Tang, X. (2017). Spatial and Temporal Variability of the PM2.5/PM10 Ratio in Wuhan, Central China. *Aerosol and Air Quality Research*, *17*(3), 741–751. https://doi.org/10.4209/aaqr.2016.09.0406

Xu, K., Cui, K., Young, L.-H., Hsieh, Y.-K., Wang, Y.-F., Zhang, J., & Wan, S. (2020). Impact of the COVID-19 Event on Air Quality in Central China. *Aerosol and Air Quality Research*, *20*(5), 915–929. https://doi.org/10.4209/aaqr.2020.04.0150

Xu, K., Cui, K., Young, L.-H., Wang, Y.-F., Hsieh, Y.-K., Wan, S., & Zhang, J. (2020). Air Quality Index, Indicatory Air Pollutants and Impact of COVID-19 Event on the Air Quality near Central China. *Aerosol and Air Quality Research*, *20*(6), 1204–1221. https://doi.org/10.4209/aaqr.2020.04.0139

Yang, J., Ji, Z., Kang, S., Zhang, Q., Chen, X., & Lee, S. Y. (2019). Spatiotemporal variations of air pollutants in western China and their relationship to meteorological factors and emission sources. *Environmental Pollution*, *254*, 112952. https://doi.org/10.1016/j.envpol.2019.07.120

Zaib, S., Lu, J., Shahid, M. Z., Ahmar, S., & Shahid, I. (2021). Impact of SARS-CoV-2 on Ambient Air Quality in Northwest China (NWC). *Atmosphere*, *12*(4), 518. https://doi.org/10.3390/atmos12040518

Zambrano-Monserrate, M. A., Ruano, M. A., & Sanchez-Alcalde, L. (2020). Indirect effects of COVID-19 on the environment. *Science of the Total Environment*, *728*, 138813. https://doi.org/10.1016/j.scitotenv.2020.138813

Zhang, J. J., Wei, Y., & Fang, Z. (2019). Ozone pollution: A major health hazard worldwide. In *Frontiers in Immunology* (Vol. 10, Issue OCT, p. 2518). Frontiers Media

S.A. https://doi.org/10.3389/fimmu.2019.02518

Zhou, Y., Wu, Y., Yang, L., Fu, L., He, K., Wang, S., Hao, J., Chen, J., & Li, C. (2010). The impact of transportation control measures on emission reductions during the 2008 Olympic Games in Beijing, China. *Atmospheric Environment*, *44*(3), 285–293. https://doi.org/10.1016/j.atmosenv.2009.10.040

Zhu, L., Jacob, D. J., Kim, P. S., Fisher, J. A., Yu, K., Travis, K. R., Mickley, L. J., Yantosca, R. M., Sulprizio, M. P., De Smedt, I., Abad, G. G., Chance, K., Li, C., Ferrare, R., Fried, A., Hair, J. W., Hanisco, T. F., Richter, D., Scarino, A. J., … Wolfe, G. M. (2016). Observing atmospheric formaldehyde (HCHO) from space: Validation and intercomparison of six retrievals from four satellites (OMI, GOME2A, GOME2B, OMPS) with SEAC4RS aircraft observations over the southeast US. *Atmospheric Chemistry and Physics*, *16*(21), 13477–13490. https://doi.org/10.5194/acp-16-13477-2016

Zhu, Y., Xie, J., Huang, F., & Cao, L. (2020). Association between short-term exposure to air pollution and COVID-19 infection: Evidence from China. *Science of the Total Environment*, *727*, 138704. https://doi.org/10.1016/j.scitotenv.2020.138704